Title

Towards new generation long trace profiler LTP-2020: system design with different sensors in different operation modes

ISBN

9781510666047

Authors

Yashchuk, Valeriy V

Anderson, Kevan

Cutler, Grant D

et al.

Publication Date

2023

DOI

10.1117/12.2677861

Towards new generation long trace profiler LTP-2020: System design with different sensors in different operation modes

Valeriy V. Yashchuk*[a], Kevan Anderson[a], Grant D. Cutler[a], Jeff Dickert[a], Damon English[a], Ralf D. Geckeler[b], Ian Lacey[a], and swflectometry[a,c]
[a]Lawrence Berkeley National Laboratory, One Cyclotron Road, Berkeley, CA 94720, USA;
[b]Physikalisch-Technische Bundesanstalt, Bundesallee 100, 38116 Braunschweig, Germany;
[c]Surface Metrology Solutions, LLC, 19 South First Street, B-901, Minneapolis, MN 55401, USA

ABSTRACT

The thorough realization of the advantages of the new generation x-ray light sources, such as the Upgraded Advanced Light Source (ALS-U) under construction, requires near-perfect x-ray optics, capable of delivering light without significant degradation of brightness and coherence. The stringent requirements of beamline optics drive the state of the art in ex situ optical metrology. Here, we present the results of the ongoing efforts at the ALS X-Ray Optics Laboratory to develop a new generation long trace profiler, LTP-2020. We discuss the system design that incorporates different types of surface slope sensors. In addition to the classical pencil beam interferometry (PBI) sensor with an improved optical design, we develop a deflectometry sensor based on a customized electronic autocollimator (AC). By applying a new data processing algorithm to the AC raw image data available from the customized AC, we significantly reduce the quasi-periodic systematic error of the AC equipped with a small size aperture. We also treat the possibility to use the AC as a PBI sensor with external light beam sources based on super-luminescent emitting diode (SLED) and single-mode laser diode (SMLD). Operation modes with stationary and/or translated sensors are possible due to the two-carriage gantry system with adjustable vertical position. The variety of the available operation modes allows optimization of the LTP-2020 experimental arrangement for providing the best possible performance in measurements with state-of-the-art aspherical x-ray optics, variable-line-spacing diffraction gratings, and multi-element optical systems.

Keywords: surface slope metrology, long trace profiler, pencil beam interferometry, angular deflectometry, electronic autocollimator, synchrotron optics, x-ray mirror metrology, diffraction grating characterization

1. INTRODUCTION

In order to thoroughly realize the potential of the new generation x-ray light sources, fully coherent free electron lasers (FELs) and diffraction-limited-storage-rings (DLSR), such as the Upgraded Advanced Light Source (ALS-U) under construction [1], we need near-perfect x-ray optics, capable of delivering light without significant degradation of brightness and coherence. The desired mirrors are often specified with residual (after subtraction of an ideal shape) surface slope and height errors of < 50-100 nrad (root-mean-square, rms) and < 1-2 nm (rms), respectively, with tight requirements to the allowed power spectral density and correlation lengths of the surface errors. For many advanced applications, such as nano-focusing and aberration-free monochromator beamlines, the desired mirrors are significantly curved in the tangential (along the beam) direction with extremely high sagittal (across the beam) curvature, presenting formidable challenges to 3D full surface metrology (for a review, see Refs. [2-6] and references therein).

Because significant x-ray reflectivity can be achieved only at small values of the grazing incidence angle, these requirements necessitate optics with lengths of the clear aperture (CA) of up to one meter in the tangential direction. The size of the beam and, correspondingly, the size of the CA in the sagittal direction is much smaller. The strong asymmetry of the geometry between the tangential and sagittal directions leads to the gravity sag effect to the mirror shape that depends on optics application in face up, face down, or side-facing deflection orientations [7-9].

The ex-situ metrology that supports the optimal configuration of these optics at the beamline must offer corresponding functionality and performance in measurements with the optics alone and, most challenging, with the optical assemblies in the arrangement as close as possible to the under operating conditions (see, for example, Refs. [10-12]).

*VVYashchuk@lbl.gov; phone 1 510 495-2592; fax 1 710 486-7696; https://als.lbl.gov/people/valeriy-yashchuk/

The peculiarities of the x-ray optics, their large size and different application arrangements, lend themselves naturally to measurements by surface profilometry, where the measurements are performed sequentially with point-by-point (subarea-by-subarea) scanning over the surface under test (SUT). This is opposite to the 'in parallel' measurement where the entire CA is mapped in a single acquisition that requires a tool with an extremely large field of view.

At the optical metrology laboratories at x-ray facilities, the most common instruments used for surface shape metrology are the surface slope-measuring deflectometers [13-32]. Surface profilometry in the height domain, such as that based on Fizeau interferometry with stitching, [33-42] appears to be much more complicated. This is due to the absolute character of the height measurements, where the sensor's height and alignment variations in the course of the sensor translation over the SUT directly contribute to the measurement error, along with retrace error that depends on the surface curvature [43]. Unlike surface profilometry in the height domain, surface slope measurements have a 'differential' character where sensors are practically insensitive to the variation of the distance between the SUT and the translating deflectometer's sensor.

The two most prevalent slope measuring instruments used to characterize x-ray optics are the long trace profiler (LTP) [14-23], using pencil beam interferometry (PBI) [44-46], and the electronic autocollimator (AC) based profilers such as the NOM (nanometer optical measuring) system at HZB/BESSY-II [24,25] and similar systems at various other facilities [26-32]. Each type of sensor has its advantages and disadvantages. The particular choice depends on the tool's intended application.

NOM-like profilers, based on different models of the most advanced industrial electronic autocollimator, the ELCOMAT 3000, [47] have been shown to be capable of very high accuracy (below 50 nrad; see, for example, Refs. [31,32]) surface slope measurements with x-ray mirrors. The accuracy achievable in the measurements with properly calibrated ACs is generally higher than that of the LTP-type deflectometers. However, the ELCOMAT AC based profilers are fundamentally unsuited for characterization of x-ray diffraction gratings. This is because of the broad-band non-coherent light-emitting diode (LED) light source used in the ACs.

Unlike the AC-based tools, the open optical layout and mechanical design of the LTP are easily reconfigurable, which allows for easier optimization of the profiler arrangement to the specifics of a particular metrology task. Thus, when equipped with a single-mode diode-laser light source, the LTP allows precision characterization of groove-density distribution of diffraction gratings [48-52]. Also, unlike the AC-based deflectometers, the LTP profilers do not require a light-limiting aperture placed close to the SUT. This simplifies measurements with optical assemblies.

The advantages of both the AC and PBI based sensors are exploited in the original HZB/BESSY-II NOM system equipped with two stationary sensors with beam folding pentaprisms placed on a translating carriage [24].

A few years ago, at the ALS X-Ray Optics Laboratory (XROL) [53], we started an R&D project on development of a new generation long trace profiler, LTP-2020, also aimed for a universality of the tool at significantly improving performance. The activity in this direction was triggered by the need for a higher performing slope measuring system suitable for high accuracy metrology on mirrors and grating for beamlines under development in the upgrade of the ALS to a DLSR facility [54,55].

Here, we present the results of the ongoing efforts on the LTP-2020 project. We discuss the system design that incorporates different types of surface slope sensors (Secs. 2 and 3). In addition to the classical pencil beam interferometry (PBI) sensor with an improved optical design [56-58] (Sec. 2), we develop a deflectometry sensor based on a customized electronic autocollimator (AC) (Sec. 3). By applying a new data processing algorithm to the AC raw image data available from the customized AC [59] (Sec. 3.3), we significantly reduce the quasi-periodic systematic error of the AC equipped with a small size aperture. We would like to treat the possibility to use the AC as a PBI sensor with external light beam sources based on super-luminescent emitting diodes (SLED) and single-mode laser diodes (SMLD) [60] (see also Sec. 2.3). In Sec. 4, we discuss the operational modes with stationary and/or translated sensors that are possible due to the two-carriage gantry system [61,62]. The variety of the available operation modes allows optimization of the LTP-2020 experimental arrangement for providing the best possible performance in measurements with state-of-the-art aspherical x-ray optics, variable-line-spacing (VLS) diffraction gratings, and multi-element optical systems. The paper concludes (Sec. 5) by summarizing the main concepts discussed through the paper and outlining a plan for future work. We would like to specially emphasize that the LTP-2020 project is welcome for new ideas and collaborations. Specifically, we encourage collaboration with others interested in the development and fabrication of the state-of-the-art optical elements and subsystems required for the superior measuring performance of the LTP-2020 system.

2. THE LTP PBI-BASED OPTICAL SENSOR OF THE LTP-2020

In this and following sections (Sec. 3), we briefly describe the design and major functionality of the LTP-2020 deflectometric sensors. Additional and more detailed and specific information is provided in Refs. [56-59].

Similar to the original BESSY-II NOM design [24], the LTP-2020 employs two different optical deflectometric sensors, a profoundly optimized LTP PBI sensor [56-58] (Sec. 2) and an electronic autocollimator sensor [59] based on a customized Moeller Wedel Optical (MWO) new flagship AC, the ELCOMAT 5000 [63] (Sec. 3).

The optical design of the LTP-2020 LTP PBI sensor incorporates improvements from the results of our extensive research and development efforts at the ALS XROL aimed at improving the performance of the LTP-II profiler that has been in continuous operation at the ALS since 1991 [64,65].

2.1 The ALS XROL LTP-II R&D as a foundation of the LTP-2020 optical sensor design

Figure 1a depicts the current schematic of the LTP-II optical sensor. It is based on the pencil beam interferometer, initially suggested and patented by K. Von Bieren in 1985 [44-46] and first applied in the long trace profiler for precision characterization of x-ray mirror surface slope topography in 1987 [14,15].

In Fig. 1a, the beam splitter BS and two Porro prisms (one movable and one stationary) constitute a phase shifter used to split the laser beam into two interfering 'pencil' beams and to adjust the phase difference and spatial separation of the beams. The polarizing beam splitter (PBS) sends the two-component beams to the SUT (the sample beam) and to the stationary reference mirror (the reference beam). By adjusting (rotating) the half-wave ($\lambda/2$) plate, one can balance the intensities of the linear polarized light in the sample and reference beams. Double pass through the quarter-wave ($\lambda/4$) plates flips the returning beams' polarizations, redirecting the reflected sample and reference beams to the Fourier transform lens (FTL) that focuses the beams onto the CCD detector chip. The focal distance of the LTP-II FTL is 1,250 mm. In order to ensure a relatively compact design of the sensor, three folding mirrors, M1, M2, and M3 are used.

Usually, the phase difference between the pencil beams is selected to be equal π, producing an interference fringe in the FTL focal plane with a minimum in the center. The position of the returned beams' intensity distributions detected with the CCD detector (e.g., that of the interference minimum or the centroid) is a measure of the angular deflection produced by reflection from the SUT and the reference mirror, respectively.

The reference arm records the spurious slope variations appearing due to carriage pitch wobbling and to pointing instability of the laser beam. Note, in the current arrangement of the ALS XROL LTP-II shown in Fig. 1a, the carriage pitch wobbling and light beam pointing instability errors contribute to the recorded sample and reference angular variations with opposite signs. Addition of a Dove prism (not shown) into the reference channel, suggested and first implemented in Refs. [64-67], changes the sign of the mechanical stage error, potentially allowing both errors to be corrected with the reference beam signal. This was extremely important for the earlier versions of the LTP tools that suffered from the low performance of the light sources that utilized non-stabilized helium–neon (He-Ne) and unstabilized single-mode diode lasers,. Pointing instability of the light beams from these sources (also due to the mode hopping) could reach 20-30 μrad. With the Dove prism added, the measurement errors could be decreased approximately by an order of magnitude, to ~3-5 μrad.

The development and implementation in our LTP-II of a multifunctional light beam source (MFLS) [60] has radically diminished the problem of the light beam pointing instability. The MFLS is comprised of a fiber coupled frequency-stabilized single-mode diode-laser (SMDL) and a superluminescent light emitting diode (SLED) light beam source (see Sec. 2.3). Implementation of the MFLS with extremely high pointing stability of the output light beam has revealed significant error in the reference arm measurements due to the fabrication imperfections in the Dove prism itself. It was also found that, with the Dove prism, there is a specific systematic error of the LTP-II reference measurements that critically depends on mutual alignment of the Dove prism and the reference mirror [21]. Because of these circumstances, we have made a new twist in the ALS LTP-II saga and returned to the original LTP PBI schematic with no Dove prism in the reference channel (Fig. 1a). Experimental tests performed with the LTP-II 'upgraded' to the no-Dove-prism optical schematic with the ultra-stable light source have demonstrated that the residual LTP-II pointing instability (still possible due to the slow temporal drift of the light source alignment) can be neglected if a multi-scan run, arranged according to an optimal scanning strategy [68,69] designed to defeat the measurement errors due to instrumental temporal drifts, is implemented.

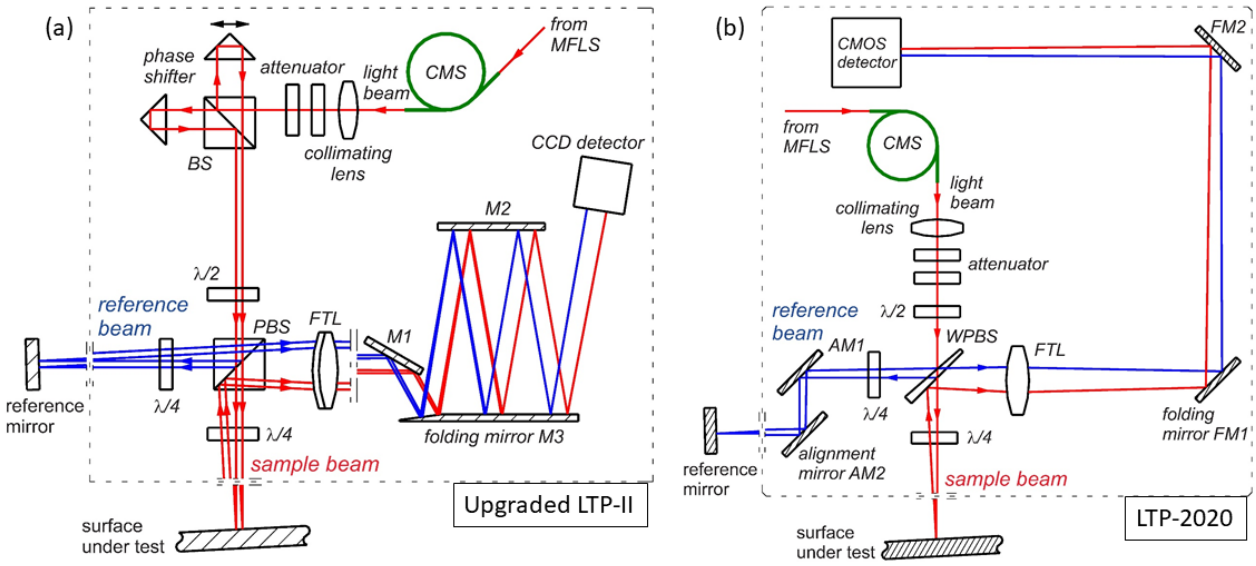

Figure 1. (a) Optical sensors of the ALS upgraded LTP-II [60] and (b) of the LTP-2020 under development. The sensor elements shown within the dotted box are placed on an air-bearing carriage that allows to translate the sensor along the surface under test (SUT) in the course of measurement. The schematics and the used abbreviations are explained in the text.

2.2 Essential additional improvements of the LTP-2020 optical sensor design

Besides the implementation of the advances in the recent upgrades of the LTP-II optical sensor, discussed in Sec. 2.1 above, the LTP-2020 optical design contains a number of modifications based on our experience characterizing the LTP-II performance and using the tool for metrology with different x-ray optics and optical systems.

A fundamental property of a slope profiler determining its operational performance is its spatial resolution, described by the instrument transfer function (ITF) (see, for example, Refs. [22,70-72] and references therein). Comparison of the spatial resolutions of the LTP-II in different operational modes is discussed in Refs. [60,72]. In particular, it is demonstrated that the spatial resolution of the LTP-II with one of the pencil beams blocked is significantly, by a factor of ~ 2, higher than that of in the classical two-pencil-beam arrangement. Based on this observation, in the optical schematic of the LTP-2020 sensor under development (Fig.1b), we use a single pencil beam.

A major source of systematic error of the LTP-II is glass inhomogeneity that introduces small phase errors into the transmitted laser beams. One of the major design criteria in the LTP-2020 is to decrease the number of optical elements and to minimize the thickness of glass in the optical path [73]. Accordingly, we have designed a wedged polarizing beam splitter (WPBS in Fig. 1b) [58] that allows us to eliminate phase error introduced into the optical path of the returned sample beam by inhomogeneity of the optical material and imperfection of the inner cemented surfaces of the LTP-II PBS cube (Fig. 1a). The wedged shape of the WPBS substrate is needed to minimize the spurious interference effects due to multiple reflections within the WPBS.

A consequence of the wedged shape of the WPBS is the non-orthogonality of the sample and reference beams that exit the WPBS. In order to ensure the parallelism of the reference beam propagating to and from the reference mirror and the sensor translation direction, we add two adjusting mirrors, AM1 and AM2 (Fig. 2b).

One of the most significant distinctions of the LTP-2020 is the Fourier transform lens that has a single element design with one surface spherical and the other aspherical. The details of the LTP-2020 FTL design and fabrication specifications based on comprehensive optical simulations are presented in Ref. [58]. Here, we would like to emphasize two major advantages anticipated with the FTL of the new design. First, compared to the two-element FTL of the LTP-II, the LTP-2020 FTL has a smaller number of optical surfaces, and it is free of an optical bonding interlayer. Therefore, we expect the overall optical quality of the new FTL to be significantly improved. Additionally, the focal length of the new FTL is 500 mm (compared to 1,250 mm of the LTP-II FTL). Therefore, instead of folding the returned beams with six reflections from three folding mirrors (Fig. 1a), we need only two reflections as depicted in Fig. 1b.

2.3 Modified multifunctional light beam source of the LTP-2020

Similar to the LTP-II, the LTP-2020 is equipped with the multifunctional light beam source allowing easy switching between operational modes utilizing the output light beams from a frequency-stabilized single-mode diode-laser and a superluminescent light emitting diode. Both SMDL and SLED are fiber-coupled and operate at the wavelengths close to that of He-Ne laser, 632.8 nm.

Figure 2 presents the LTP-2020 MFLS schematic that is slightly modified compared with the LTP-II version described in detail in Ref. [60].

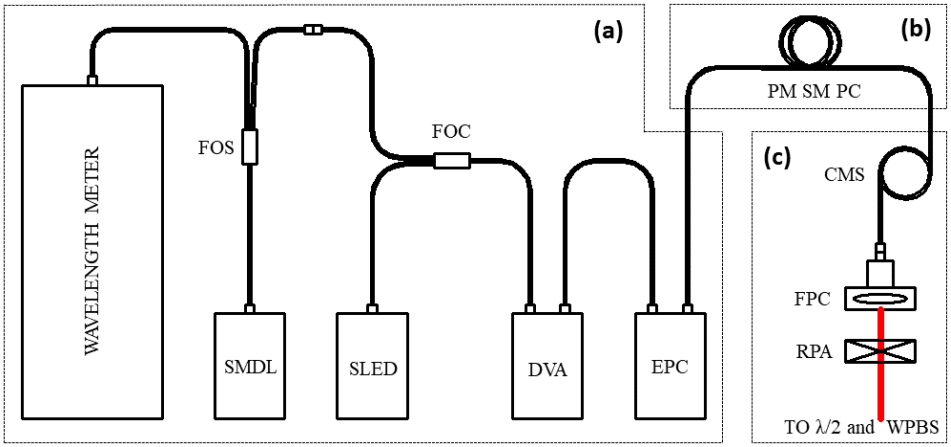

Figure 2 Schematic of the multifunctional light source: the elements placed (a) stationary on the LTP-2020 optical table, (b) in the folding tray, and (c) on the movable carriage. SMDL is the single longitudinal mode fiber-coupled diode laser, SLED is the superluminescent light emitting diode module; DVA is the digital variable attenuator; EPC is the electronic polarization controller; FOS is the 630-nm 1×2 single mode fiber optic splitters with splitting ration 90:10; FOC is the 630 nm 2×1 single mode fiber optic coupler with coupling ration 50:50; PM SM PC is the polarization-maintaining single-mode patch cable; CMS is the cladding mode suppressor made of 7 loops of the patch cable; FPC is the fiber-port collimator with five degrees of freedom plus rotation adjustment; RPA is the rotating polarizer attenuator. After the RPA, the light beam goes to the lambda/2 plate and wedged polarizing beam splitter WPBS of the LTP-2020 optical sensor (see also Fig. 1b).

Working with the LTP-II equipped with the MFLS, we have found that the power and polarization direction of the light exiting the polarization-maintaining single-mode patch cable (PM SM PC in Fig. 2) are slowly varying [60]. This is due to the continuous bending of the PM SM PC in the course of translation the LTP-II sensor. Such bending of a fiber cable is known to cause so-called 'bend losses' of the light power (see, for example, Refs. [74,75] and references therein). This is due to the coupling of the light from core modes (guided modes) to cladding modes, when the fiber is bent. In the LTP application, the position of the fiber bending varies on the scale of a few meters, which can lead to a significant fluctuation of the power and polarization of the output light. The power fluctuation can be suppressed with addition of a cladding mode suppressor that, in our case, is a stationary loop in the downstream part of fiber of 5-10 turns, labeled in Fig. 2 as 'CMS.' Unfortunately, the output light intensity stabilization with the CMS is not perfect. Because of this, we adopt an active stabilization of the light-beam intensity with the digital variable attenuator (DVA) in the LTP-II MFLS system [60]. The stabilization that uses the integrated intensity of the detected light as a feedback signal is one of the functions of the LTP-2020 motion control and data acquisition (MCDA) system under development.

The variation of the light polarization direction leads to a change of the light intensity after the two-polarizer attenuator (Fig. 1). In the LTP-II, the compensation of the spurious effect of the polarization direction variation is performed manually by simultaneously adjusting the attenuator and the half-wave plate (Fig. 1). In order to enable a remote (and automated) compensation, in the MFLS schematic for the LTP-2020 shown in Fig. 2, we have added the rotating polarizer attenuator (RPA). In this case, as a feedback signal for the polarization stabilization, the LTP-2020 MCDA system uses the normalized difference of the integrated intensities of the sample and reference light beams:

$$PFS = \left(I_S - I_R\right)/\left(I_S + I_R\right), \tag{1}$$

where PFS is the polarization feedback signal, I_S and are I_R the integrated intensities of the detected sample and reference light beams, respectively.

The MCDA system also provides for automated control and monitoring of all major parameters of the SMDL, SLED, and DVA. In the case of the SMDL light beam used for metrology with x-ray gratings, we additionally record in the measurement data file the temporal variation of the light wavelength measured with the wavelength meter [76] (Fig. 2) that is specified to measure the absolute wavelength with an accuracy of ± 0.0008 nm (see also Sec. 4).

Concluding the overview of the MFLS, we should note that the newer models of the SMDL and SLED with the output light power of ~ 5 mW are implemented in the LTP-2020. This should be compared to 3 mW in the models currently in use in the LTP-II. The availability of the higher light power is beneficial for measurements on x-ray mirrors with low reflectance coatings (such as, for example, carbon coatings) over the visible light spectrum.

With the MFLS source (Fig. 2), the LTP-2020 can be easily reconfigured for measurements of x-ray mirrors or diffraction gratings. Usage of a light beam with a low degree of coherence for mirror metrology helps to suppress the LTP systematic errors due to spurious interference effects in the LTP optical elements (for a comprehensive discussion of the LTP-2020 systematic errors due to spurious interference effects, see Refs. [56-58]). The high-coherence narrow-band light beam is used for groove-density-distribution characterization of x-ray diffraction gratings. The measuring advantages of the various arrangements of the LTP-2020 possible with different types of light beam sources and data acquisition methods are discussed in Sec. 4.

2.4 Selection of a CMOS camera for the LTP-2020 detector

In the current version of the LTP-II sensor, we use the Lumenera Lt29059HM-WOCG camera without the sensor cover glass. The camera is based on the KAI-29050-NIR CCD image sensor with the number of active pixels of 6576 × 4384 with the pixel size of 5.5 μm × 5.5 μm. The camera has a glass window with a broadband antireflection coating. The temperature of the camera body is stabilized at 23°C (at the lab room temperature of 21°C) with a homemade Peltier cooler mounted directly to the camera body with an indium spacer.

The no-cover-glass customization solved the potential problem of the beam image distortion due to the interference of the direct light and the light reflected from the image sensor and back-reflected from the cover glass. However, such kind of image distortion is still present due to the back-reflection effect associated with the camera glass window. This is illustrated in Fig. 3 where the images of the sample beam reflected from an SUT at three different slope angles with the total variation of ~8.2 mrad are shown as recorded with the LTP-II CCD camera.

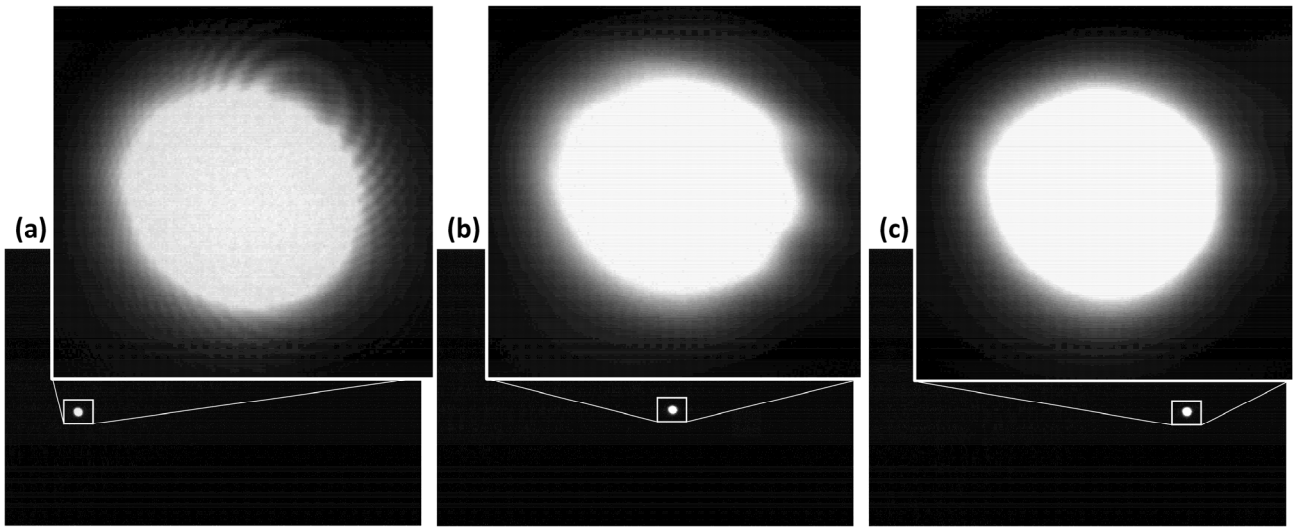

Figure 3. Images of the LTP-II SMDL sample beam recorded with the Lumenera Lt29059HM-WOCG camera image sensor at the beam intensity producing a strong oversaturation of the central area of the beam image, and exaggerating the periphery of the beam footprint. The images (a), (b), and (b) correspond to the SUT mirror tilts with the total difference of about 8.2 mrad. The interference pattern of the back-reflection distortion around the central oversaturated beam footprint is seen in plot (a).

The intensity of the beam imaged in Fig. 3 was specially increased to oversaturate the central area, while amplifying the periphery of the beam footprint with relatively weak interference artifacts. Thus, the interference pattern of the back-reflection distortion of the beam image is seen in the Fig. 3a, where the maximum slope angle with respect to the almost normal incidence to the camera window in Fig. 3c, where the image looks to be almost free of the interference distortion.

The intensity of the spurious interference pattern strongly depends on the quality of the antireflection coating. The beam image perturbation could still be acceptable if the distortion pattern stays constant during the slope measurements with a curved x-ray optics. However, the data in Fig. 3, as well as the numerical simulations performed in Ref. [58], have revealed a strong dependence of the interference distortion on the incidence angle of the recorded light beam. In the LTP-II application to the surface slope metrology, this leads to a specific systematic error that is a function of the shape and angular alignment of the SUT. Therefore, we should put special attention to the quality of the AR coating on the glass window and on the image sensor cover glass if they cannot be totally removed.

Unfortunately, when searching for a high-quality camera for the LTP-2020 detector, we found that the market of suitable cameras with a possibility to customize a high-quality AR window coating is extremely narrow. To the best of our understanding, there are two major reasons for this difficulty. First, the market has sharply moved from CCD image sensors to CMOS sensors. As a result, we could not find a Lumenera Lt29059HM-WOCG or a similar camera because they are no longer available on the market. Second, most of the modern cameras based on the CMOS image sensors are designed with a microlens array needed to increase the light detection efficiency. As we have seen in a number of tests on cameras with the microlens array, the back-reflection distortion of the beam intensity pattern produces unacceptable spurious interference.. Fortunately, there is an extremely narrow market of scientific grade CMOS cameras available free of the microlens array. These cameras are based on backside illuminated CMOS image sensors that have significantly larger pixel sensitive areas than that of the front illuminated ones.

Currently, we are working on customizing the specification for a Teledyne Kinetix scientific CMOS (sCMOS) camera with a 10 Mpixel back-illuminated image sensor with a pixel size of 6.5 μm x 6.5 μm [77]. It has a 1 mm thick fused silica window located 10 mm in front of the sensor. Based on the numerical simulations discussed in Ref. [58], the AR coating on both sides of the window needs to have a maximum reflectivity of 0.01% at 633 nm to ensure the distortion of the recorded beam position below the 30 nrad level. We are currently working with a coating vendor to develop a suitable AR coating for the fused silica window. Note that as an sCMOS camera, the Kinetix is much faster than the LTP-II CCD Lumenera camera. The need to speed up the deflectometric measurements with VLS gratings is one of the imperatives of the LTP-2020 project.

3. LTP-2020 SENSOR BASED ON A CUSTOMIZED AC ELCOMAT 5000

Most, if not all, AC-based surface slope profilometers in use in the metrology laboratories at x-ray facilities are based on the different models of the ELCOMAT series autocollimators made by Moeller Wedel Optical [47,63] (see also Sec. 3.1). At the ALS XROL, we routinely use two AC based profilometers: Developmental LTP (DLTP) [26,30] and Optical Surface Measuring System (OSMS) [32,78,79]. Both our profilometers utilize AC ELCOMAT 3000 [47] precisely calibrated at the Physikalisch-Technische Bundesanstalt (PTB), Germany, using a sophisticated experimental method and set-up [80-82]. In Sec. 3.2 on the example of the DLTP and OSMS, we outline the two major deflectometry applications of the ACs as the stationary and movable sensors. Our experience developing and exploiting DLTP and OSMS is a basis for the development of the LTP-2020 operation arrangements with the AC sensor considered in Sec. 4.

In the LTP-2020, we plan to use a customized version of the MWO new flagship AC, the ELCOMAT 5000 [63]. The customization enables automatic recording of the AC raw image data and complete control of the built-in light source intensity. Access to the AC raw image data allows us to apply different data processing algorithms with the goal of reducing the measurement systematic errors in a particular AC operation arrangement. Thus, we have recently developed and demonstrated a correlation analysis based algorithm that, in application to the raw image data recorded with the AC ELCOMAT 3000 in the surface slope deflectometer arrangement, allows to significantly (by a factor of 4-5) reduce the AC quasi-periodic systematic error [59] (see also Sec. 3.3). As a plan for the near future, we would like to investigate a possibility to use the AC as a PBI sensor with different external light beam sources based on the SLED and SMLD discussed in Sec. 2.3, above.

3.1 Application of ELCOMAT electronic autocollimators to surface slope profilometry

In this section, we discuss the optical design and major technical parameters of the ELCOMAT 3000 [47] in application to the surface slope profilometry. Figure 4 presents an optical schematic diagram of the ELCOMAT autocollimator.

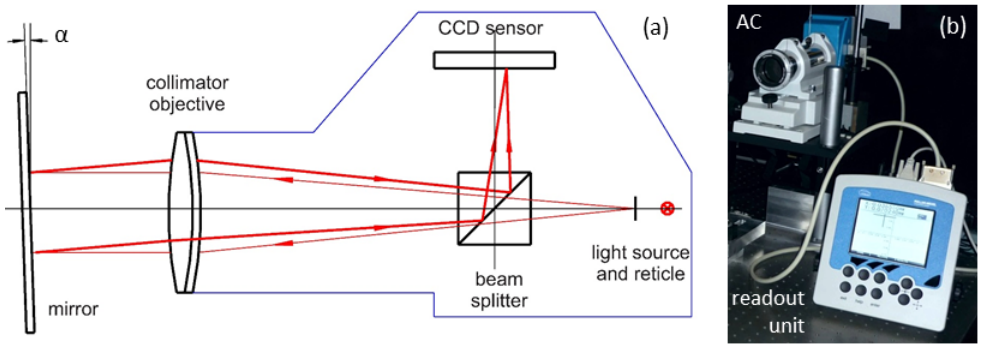

Figure 4. (a) Optical schematic diagram and (b) a picture of the ELCOMAT 3000 autocollimator. The AC has a closed design with the elements as depicted in plot (a) within the blue-lined box. See text for details.

Similar to the LTP PBI sensor (Sec. 2.1), angle measurement of an autocollimator is based on assessing the shift of the reflected light intensity distribution (the reticle image) recorded with a CCD detector. However, the autocollimator's objective lens has two functions. First, it collimates the outgoing light beam directed to the mirror (Fig. 4). Second, it serves as an FTL in the PBI sensor linearly transforming the angular deflection of the reflected beam into a measurable image position shift.

According to the specifications [47], the best performance of the ELCOMAT 3000 is achieved with a large aperture diameter of the outgoing beam. The specified minimum diameter is 5-6 mm depending on the AC application. For surface slope profilometry, a circular aperture with a diameter of about 2.5 mm diameter is typically used [83,84]. In order to minimize the reflected beam shape distortion, the aperture is placed close to the SUT, usually within ~ 3 mm or less.

With the optimally aligned 2.5-mm aperture [85], the spatial resolution of the OSMS corresponding to the first zero-crossing of the instrument transform function (ITF) is about 1.4 mm as measured with a specially developed test sample with chirped surface slope profiles [70,72]. The performance of the AC deflectometer with differently shaped apertures has been investigated in Ref. [79]. A significant resolution improvement was demonstrated, by a factor of about 1.4, with a rectangular aperture with the size of 1.5 mm (tangential) × 3 mm (sagittal).

Note that systematic error of the measurements with the AC based deflectometer strongly depends on the size and shape of the aperture [79], as well as on the environmental conditions and operation mode of the deflectometer with a stationary or a movable AC [59,82,83,86,87] (see also discussion in Sec. 3.2, below).

As mentioned above, in the LTP-2020 we plan to use a customized version of the new MWO autocollimator ELCOMAT 5000. According to the specification [63], the ELCOMAT 5000 has a significantly larger measuring range of ± 7.3 mrad compared to that of ± 4.8 mrad available with the ELCOMAT 3000. The optical electronic design of the ELCOMAT 5000 allows for a 10-fold higher measurement frequency, 250 Hz, at the same specified accuracy, resolution, and reproducibility. Together with an additional function of time analysis of the measured values, the higher measurement frequency makes much more practical implementation of the "on-the-fly" mode of measurements [27,88]. A very hands-on advantage is the easy, fast and precise adjustment/alignment of the ELCOMAT 5000 autocollimator that is possible with additional internal alignment sensors in the autocollimation sensor [63] (see also a relevant discussion in Ref. [89]).

3.2 The ALS XROL surface slope profilers based on electronic autocollimators ELCOMAT 3000

The ALS DLTP [26,30] is a relatively low cost realisation of a deflectometric profilometer based on an industrial electronic autocollimator and a movable pentaprism – Fig. 5. This optical schematic was first suggested and realized at the PTB by E. Debler and K. Zander in 1978-1980 [90] and K. von Bieren in 1985 [46]. Later on, the movable pentaprism mode of operation was adapted to an LTP with a stationary optics sensor [91]. The major advantage of the movable pentaprism profilometry is the suppression of the carriage wobbling error.

Figure 5 shows the DLTP in two different arrangements suitable for surface slope metrology with the SUTs in the face-up (Fig. 5a) and (Fig. 5b) side-facing orientations. In order to change the arrangement, there are two sets of the mirror-based pentaprisms (Fig. 5c) that are easily interchangeable. The application of the mirror-based pentaprisms allows us to

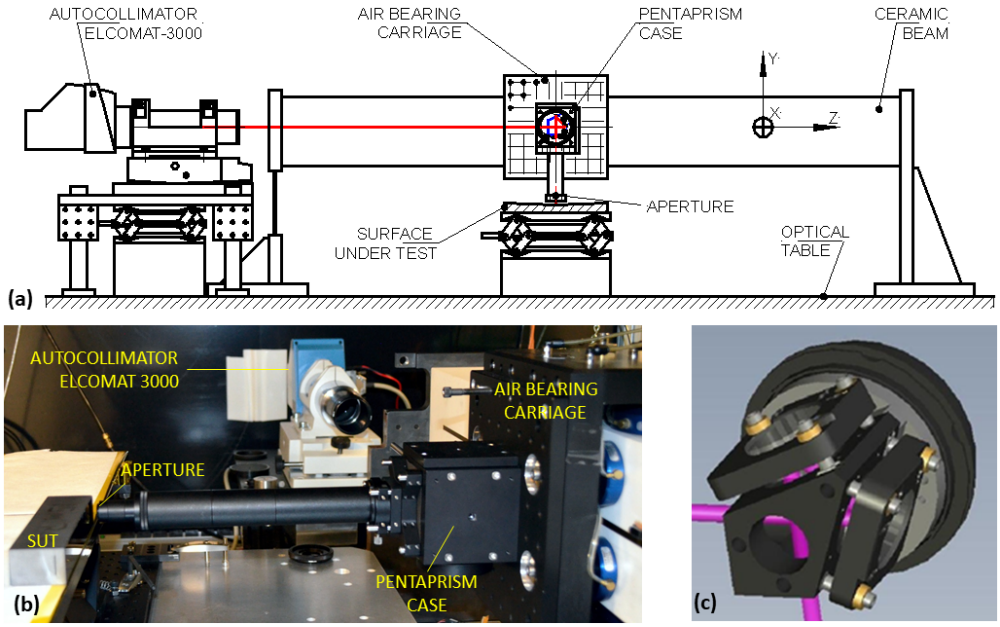

Figure 5. (a) Optical schematic diagram and (b) a picture of the ALS XROL DLTP; (c) design of the DLTP mirror-based pentaprism. In plot (a), the DLTP is depicted in an arrangement for metrology with a SUT in face-up orientation; whereas, in plot (b), the DLTP is pictured as set for measurements with a SUT in side-facing orientation. See text for more details.

avoid the optical path perturbation due to the optical material inhomogeneity usual for the solid glass pentaprisms. Additionally, the mirror surface quality can generally be much better than the effective quality of the four surfaces of a glass pentaprism. The design and the methodology for precision assembly and alignment of the mirror-based pentaprisms are described in detail in Refs. [92,93].

In the deflectometric profilometers like the DLTP, which use a movable pentaprism to scan the SUT, the effective distance to the SUT (that is the autocollimator beam length) is unavoidably changing. If there is an error of the AC detector (sensor) location with respect to the focal plane of the autocollimator's objective, the AC-SUT distance variation leads to an angle error, which depends on the distance (see the relevant discussion in Ref. [87], as well as in the references therein):

$$\delta\alpha = \left(L/f_0 - 1\right)\cdot\left(1 - D/f_0\right), \tag{2}$$

where f_0 is the focal length of the autocollimator's objective, D is the AC-SUT distance, L is the detector position with respect to the focal plane of the AC objective. Because the objective's focal length depends on the refractive indexes of the air and the objective's lens glass changing with the temperature, pressure, and humidity of air, the AC-SUT distance dependent error [Eq. (2)] appears to be very difficult to calibrate and reliably account for in the measurement result.

For the autocollimators ELCOMAT 3000 and ELCOMAT 5000, $f_0 = 300$ mm. Therefore, in the measurements with long grazing incidence x-ray mirrors, the absolute value of the second term in Eq. (2) can be significantly larger than 1, whereas the detector positioning term is many orders of magnitude smaller than 1. This opens an efficient way for, practically, elimination of the AC-SUT distance dependent error. Indeed, for

$$\left(f_0 - D\right)/f_0 << 1, \tag{3}$$

the error given by Eq. (2) can be neglected.

Figure 6a depicts a schematic of a profilometer, realizing this possibility [94]. It has a movable AC based sensor and an additional reference AC to monitor the wobbling error of the main (sample) AC translation. This schematic that is basically equivalent to the LTP with movable sensor, is now realized in a number of AC-based surface slope profilometers at different x-ray facilities (see, for example, Refs. [28, 95-97] and references therein). This includes the OSMS at the ALS XROL [32,78,79] depicted in Fig. 6b.

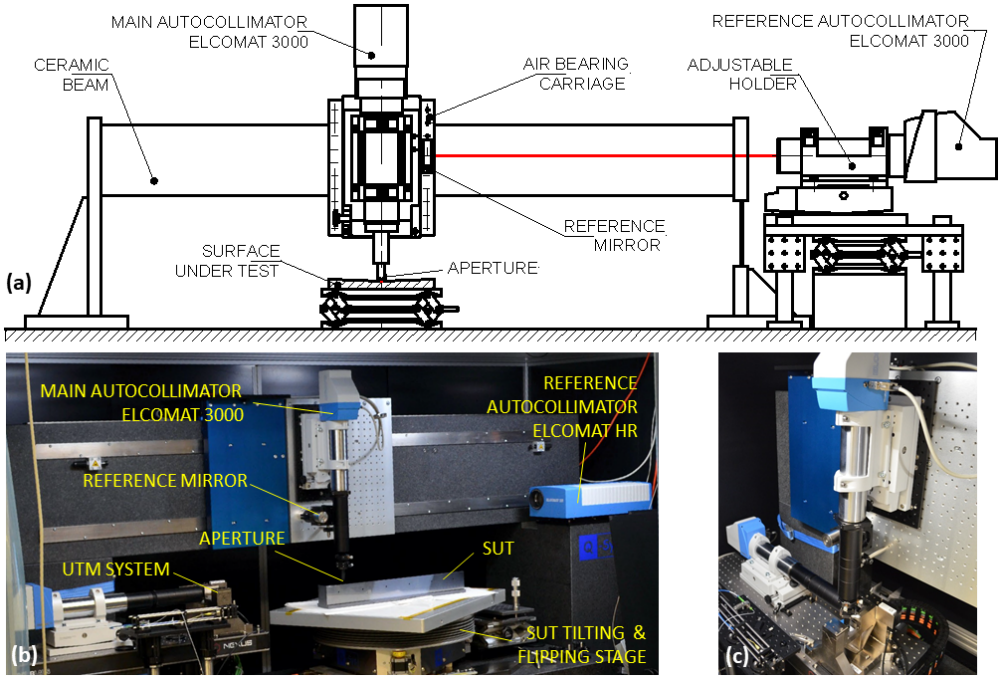

Figure 6. (a) Optical schematic diagram and (b) a picture of the ALS OSMS designed for surface slope metrology with a SUT in face-up orientation; (c) the OSMS main autocollimator as placed for calibration with the Universal Test Mirror (UTM) system [98,99]. See text for more details.

The ALS OSMS (Fig. 6) is designed for surface slope metrology with a SUT in face-up orientation with the aperture mounted to a cage tube at ~ 297 mm from the autocollimator's objective. At the distance between the aperture and the SUT of ~ 3 mm, $D \simeq f_0$ ensuring the condition (3) and, therefore, a negligibly small contribution of the AC-SUT distance dependent error given by Eq. (2). The reference autocollimator ELCOMAT HR is directed to a reference mirror mounted on the carriage (Fig. 6b) and monitors the carriage wobbling error.

The constraint and close to optimal AC-SUT distance opens a possibility to transfer to the main AC the high accuracy angular calibration of a 'standard' AC preliminary calibrated at the PTB. This possibility is realized in the OSMS with the Universal Test Mirror (UTM) system [98,99] (Fig. 6b). Figure 6c depicts the OSMS arrangement when the main autocollimator is placed for calibration transfer with the UTM.

Concluding this section, we should acknowledge the principal difference between the data acquisition methods applied to the OSMS and DLTP measurements for the high accuracy characterization of state-of-the-art x-ray mirrors. Due to the SUT tilting and flipping stage integrated to the OSMS (Fig. 6c), the OSMS completely employs the data acquisition method based on the advanced optimal scanning strategy (AOSS) [68,69] that allows for suppression of the measurement errors related to the AC systematic error and the instrumental and set-up drifts. Application of the AOSS to the LTP-2020 measurements when using, for example, the automated rotating/flipping/aligning (ARFA) system [100] should also be beneficial for suppression of the tool's systematic and drift related errors.

3.3 Development of an original algorithm and software for reprocessing of the AC raw data

The accuracy of the measurements with the AC-based profilometers is mostly limited by the specific systematic errors of the AC used. In addition to errors caused by geometric aberrations in the imaging of the reticle by the objective, quasi-periodic errors occur on angular scales corresponding to the dimensions of the structures of the reticle pattern and the size of the pixels of the CCD detector. The magnitude of the systematic errors is highly dependent on the data processing algorithm applied to the captured reticle image.

As mentioned above, in the LTP-2020, we plan to use the MWO new AC ELCOMAT 5000 customized to enable, in particular, automatic recording of the AC raw image data. A possibility for a significant improvement of the angle measurement accuracy by use of advanced algorithms for the analysis of the reticle images recorded with a customized

AC ELCOMAT 3000 have been recently demonstrated in Ref. [101]. Here, we just briefly outline the basic idea in the foundation of the developed algorithm and software discussed in detail in Ref. [59].

The basic idea of the method (Fig. 7) consists in the use of a cross-correlation (covariance) analysis with a reference image (recorded, for example, at the center of the measurement range) for the precise determination of the position (localization) of the recorded images. Before calculating the covariance function, both images are resampled by interpolating the images taken with the AC detector pixelation to a denser grid with an increased number of subpixels. The combination of cross correlation and interpolation allows increasing the sensitivity to the mutual position shift in the matching of the reticle image under test with the reference image. The shift of the cross-correlation function evaluated from the reticle intensity distributions of the reference and the scanning (measurement) angle of the SUT (Fig. 7) is a measure of the SUT tilt angle.

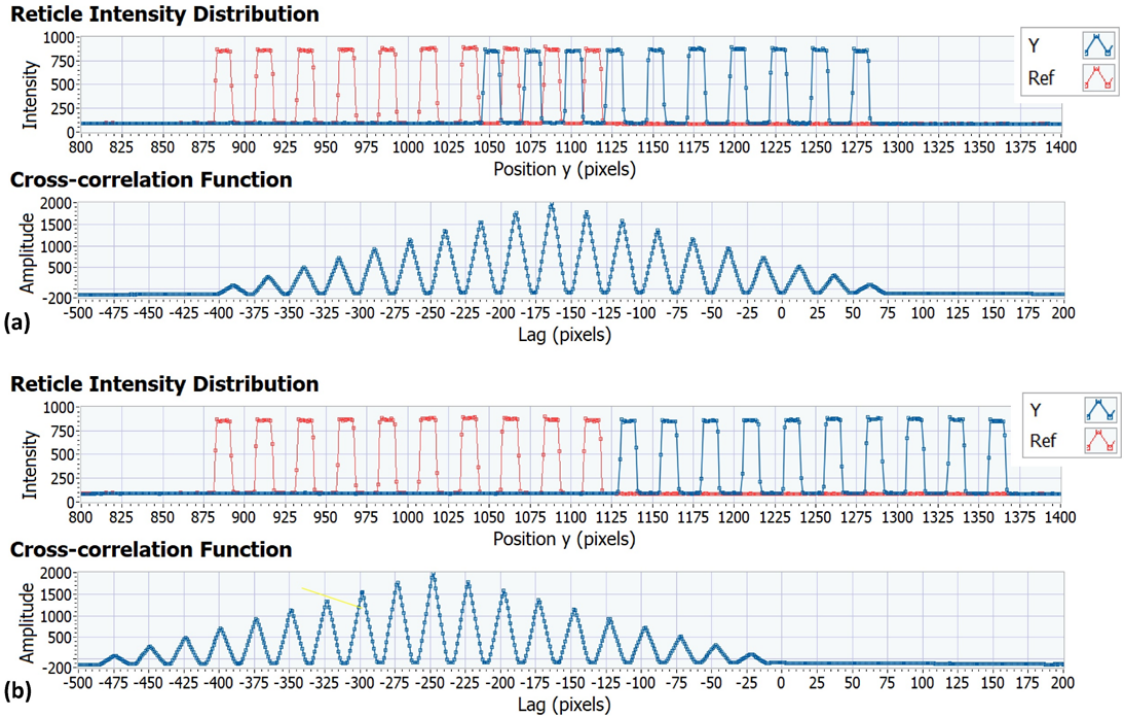

Figure 7. (a) Reticle intensity distributions recorded with the AC CCD detector at the reference angle and at a scanning (measurement) angle (the red and blue dotted traces in the top plot, respectively) and (the bottom trace) the cross-correlation function of the reference and scanning distributions in the top plot. (b) The same data as in (a) but with the scanning distribution taken at different tilt of the SUT.

As a proof-of-concept, we have compared the results of the application of the new and built-in data processing procedures to reticle image data, recorded during the calibration of a commercial autocollimator, performed at the PTB. A numerical criterion for the efficacy of the data processing procedures under comparison is the deviation of the processed slope traces from the trace of the reference mirror tilt angles preset with PTB's primary angle standard WMT 220 used for the calibration [80,102].

Figure 8a shows the original calibration trace of an AC ELCOMAT 3000 presented as an angular dependence of the difference between the reference mirror tilt angle recorded with the AC and the actual angle preset with the WMT 220. The AC under calibration was equipped with an aperture with 2.5 mm diameter placed at ~ 3 mm in the front of the reference mirror located at the 300 mm distance from the AC's objective.

The overall amplitude of the calibrated AC error in Fig. 8a is about ± 1.2 µrad. The error has a strong low angular frequency component with the period of about 7.3 mrad. There is also a clearly visible higher frequency component with the amplitude of ~ 0.4 µrad and the period of ~ 300 µrad. Note that the AC's built-in routine for evaluation of the recorded angle is optimized by the manufacturer for AC applications with apertures much larger than 2.5-mm diameter aperture used here which is typical for the AC application in surface slope profilometers.

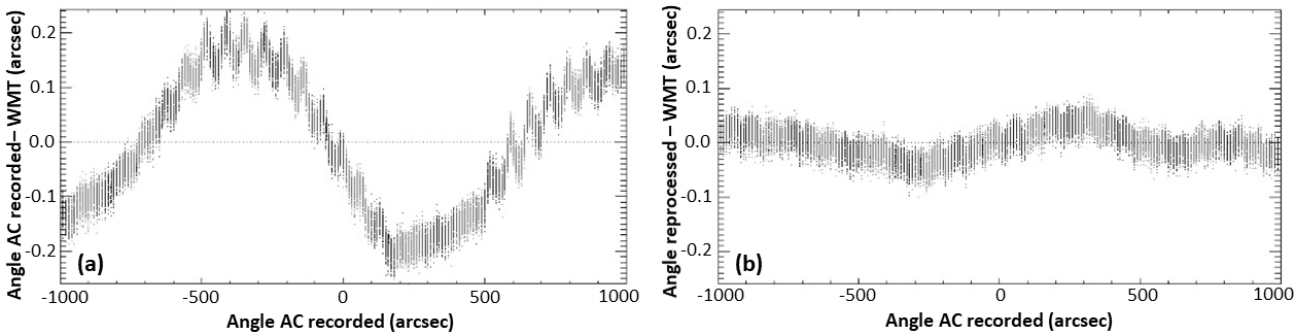

Figure 8. (a) The original calibration trace of an AC ELCOMAT 3000 presented as an angular dependence of the difference between the reference mirror tilt angle recorded with the AC and the actual angle preset with the WMT 220. (b) The calibration trace obtained with the same data but retreated with the developed algorithm for processing reticle image data [59]. The AC under calibration was equipped with an aperture with 2.5 mm diameter placed at ~ 3 mm in the front of the reference mirror located at the 300 mm distance from the AC's objective.

The calibration trace obtained with the same data, but reprocessed with the developed algorithm for processing reticle image data as described in detail in Ref. [59], is presented in Fig. 8b. The reprocessing makes it possible to significantly reduce the magnitude of systematic errors in the AC applications in profilometry. Indeed, the amplitude of the low frequency error is decreased by a factor of 4-5 when compared to the AC's built-in routine (Fig. 8a). Moreover, the higher frequency component with the period of ~ 300 μrad is now at a level below the measurement noise.

Concluding this section, we would like to emphasize that our correlation analysis approach suggested and demonstrated for processing AC reticle image data with significantly reduced systematic errors is applicable also to other cases where the light intensity distribution of a sampling light beam is mapped by an objective (such as an FTL in the LTP sensor) onto a pixelated detector. The technique has the potential to improve the localization (positioning) of structures and edges in pixelated images in general, and the experimental verification of the technique using the reticle images of an autocollimator is just a specific use case.

4. MODES OF OPERATION POSSIBLE WITH THE LTP-2020

One of the most significant differences of the LTP-2020 from all other deflectometry tools in use at the x-ray facilities is the two-carriage gantry system depicted in Fig. 9a and discussed in detail in Refs. [61,62].

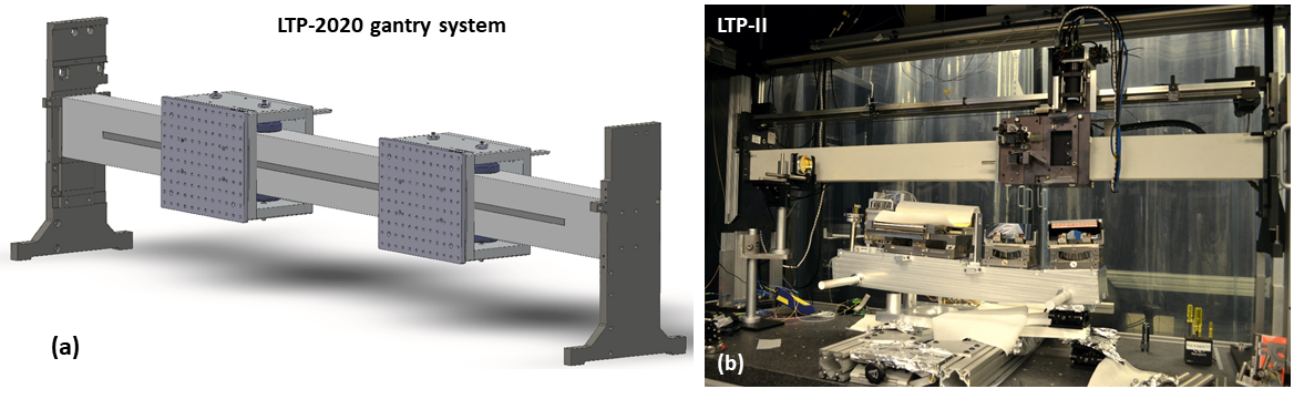

Figure 9. (a) General design view of the LTP-2020 two-carriage gantry system. (b) The LTP-II arrangement with a single carriage gantry system designed with a capability for raising the LTP sensor above the optical bench to increase the space needed for measurements of large multi-component optical assemblies. See text for more details.

The design of the LTP-2020 gantry system carriages is similar to that of the DLTP [26]. These are two identical carriages with air-bearing suspension. The carriages are driven by piezoceramic ultrasonic motors allowing to translate

each carriage along a ceramic beam over a distance of approximately 1 m. Linear encoders provide positioning of each carriage with a specified accuracy of ~ 0.1 μm. The data acquisition rate feasible with the LTP-2020 gantry system in the move-stop-measure mode of operation is the same as for the DLTP (~ 3 sec) and a factor of ~ 5 higher than the rate possible with the current LTP-II (~ 16 sec) which has a very slow CCD detector and a carriage driven with a metal belt.

The design specifications of the LTP-2020 gantry system in Fig. 9a [61,62], including the dimensions of the ceramic beam and its mechanical support assembly, are the same as those of the LTP-II. The similarity of the designs is intentional allowing replacing the LTP-II with the LTP-2020, when the latter is brought into operation. With the LTP-2020 two-carriage gantry system, it becomes possible to provide a broader assortment of the operation modes with stationary and/or translated sensors. This allows for the possibility of better matching (optimizing) of the LTP-2020 operation mode to the specific metrology task and the measurement arrangement. At the same time, the replacement would preserve the unique property of the ALS XROL LTP-II gantry system, illustrated in Fig. 9b, which is a capability for raising the LTP sensor above the optical bench to increase the space needed for measurements of large multi-component optical assemblies [14-17].

Below in this section, we outline the major measurement arrangements and operation modes of the LTP-2020 exploiting two optical deflectometric sensors, the optimized LTP PBI sensor and the AC sensor based on the customized ELCOMAT 5000 described in Sec. 2 and Sec. 3, respectively.

4.1 X-ray mirror metrology with the LTP-2020

Figure 10 sketches the LTP-2020 setup arranged for measuring two different mirrors. One mirror is placed for measurements with the stationary AC and movable pentaprism that is the NOM- and DLTP-like operation mode shown in Fig. 5 and discussed in Sec. 3.2. The other mirror is under measurements with the LTP-2020 PBI sensor depicted in Fig. 1b. This mode of operation is generally the same as that of the current LTP-II (compare with Figs. 1a and 9b). In order to ensure the maximum scanning range in both arms, the reference mirror can be placed as shown in Fig. 11.

In both operation modes sketched in Figs. 10 and 11, the LTP-2020 is expected to provide a significantly higher accuracy relative to the DLTP and LTP-II due to the improved PBI and AC based sensors described in Secs. 2 and 3, respectively.

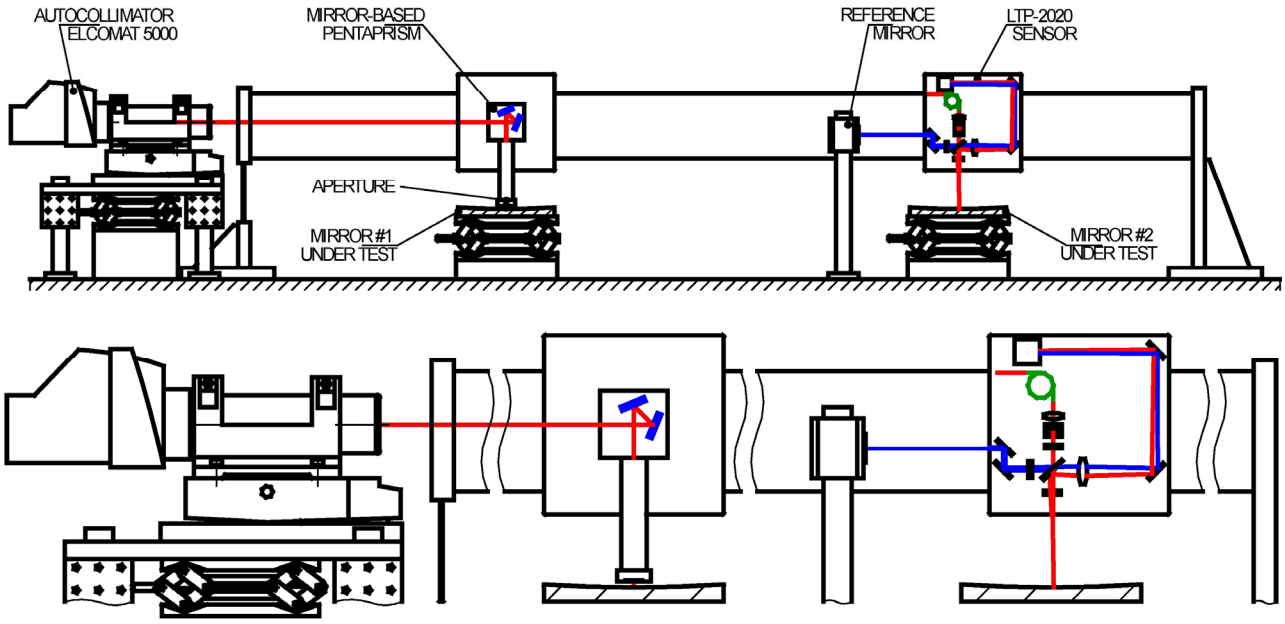

Figure 10. The LTP-2020 setup arranged for measuring two different mirrors (the bottom enlarged sketch is for clearness). One mirror under test (#1) is placed for measurements with the stationary AC and movable pentaprism, and the other mirror (#2) is under measurements with the LTP PBI sensor of the LTP-2020. These modes of operation are generally the same as that of the current ALS XROL DLTP and LTP-II.

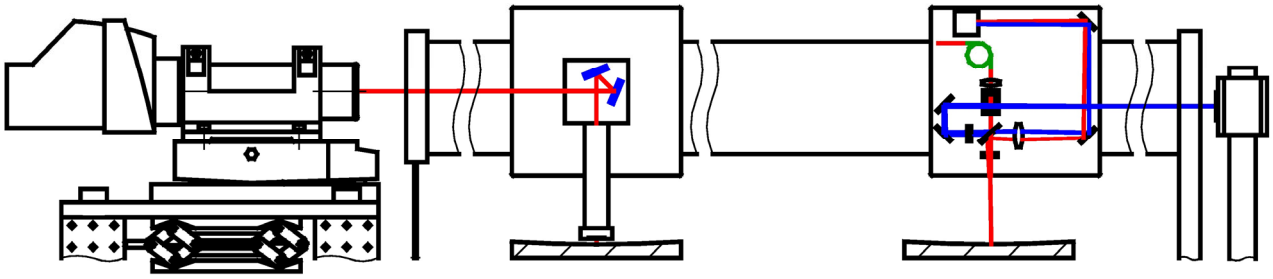

Figure 11. The LTP-2020 setup for measuring two different mirrors with the maximum scanning range in both arms.

An additional advantage of the LTP-2020 is that the two measurements shown in Figs. 10 and 11 can be performed simultaneously. In order to realize this option, the profiler motion and control system has to support a synchronized move-stop-measure mode of the data acquisition in the both arms. The synchronization is needed in order to avoid a distortion of the measurements in one arm due to the carriage motion in the other arm.

The LTP-2020 PBI sensor in Figs. 10 and 11, with the single reference mirror mounted off the moving optical head, is subject to two significant error sources in the reference beam: one is mechanical errors due to jitter in the carriage motion and also to temporal instabilities, and the other is laser beam pointing instability. These errors are exactly out of phase, so that correcting for one doubles the other. In order to eliminate this problem, we can rearrange the measurement arrangement with the PBI sensor as sketched in Fig. 12, adding a second reference mirror and placing both onto the optics board. In both setups shown in Fig. 12, the AC is used to monitor the wobbling of the carriage with the LTP-2020 PBI sensor by recording the variation of the angular position of the reference mirror 1. Reference mirror 2 is placed in the sensor reference channel to monitor the light beam pointing instability. In order to ensure the maximum flexibility of the LTP-2020 setup, we plan to use an additional AC in the position shown in Fig. 12 b.

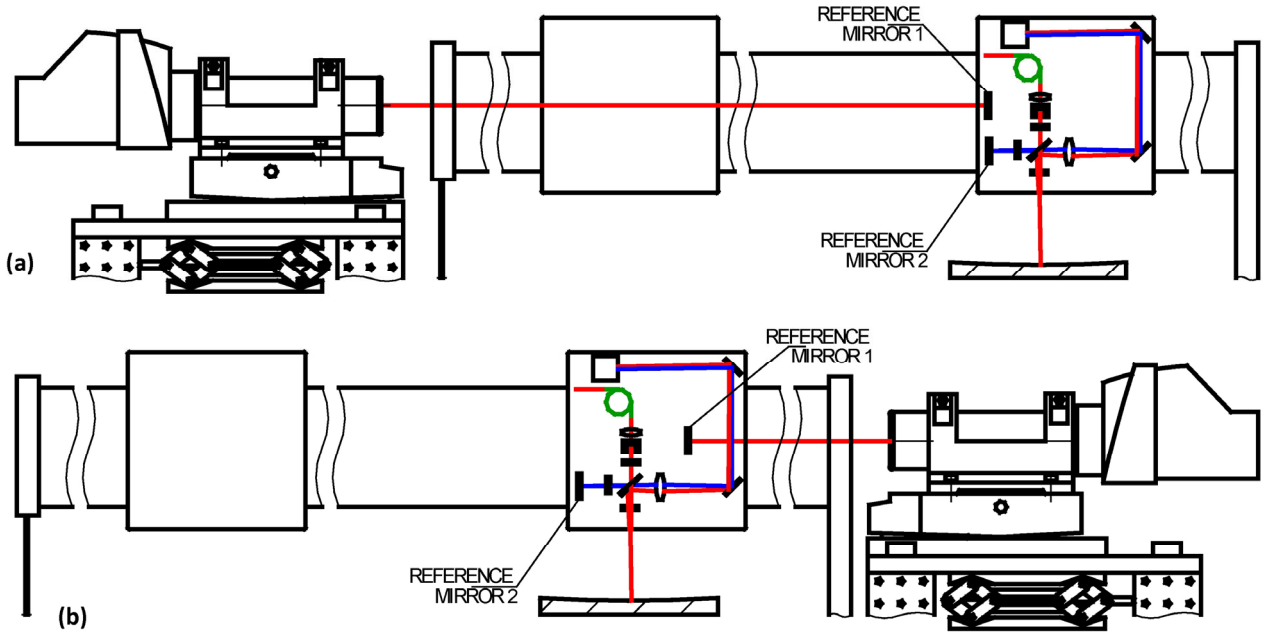

Figure 12. Two possible arrangements of the LTP-2020 setup for high accuracy measurements with the LTP-2020 PBI sensor with simultaneous monitoring (recording) of the carriage wobbling and light beam pointing instability (a) with the main AC and (b) with an additional AC.

As an example of the LTP-2020 application to the measurements of multi-element optical systems, Fig. 13 depicts the LTP-2020 experimental arrangement optimized for alignment and measurements with an optical assembly of a one-dimensional (1D) Wolter Type I optical system consisting of a pair of mirrors, one hyperbolic and one elliptical [103,104]. Such optical system, for example, is a part of the QERLIN (the double-dispersion RIXS instrumentation)

spectrometer under development at the ALS beamline BL 6.0.2 [105,106]. The desired relative pitch tilt of the mirrors in the QERLIN spectrometer is $\gamma = 4$ degrees that is much larger than the angular dynamic range of any ALS XROL profiler. Therefore, the metrology with the Wolter pair assembly is associated with a realignment of the system between the measurements over different mirrors. The realignment is a rather time-consuming complicated procedure, difficult to perform with the required accuracy on the level of ~ 40 μrad.

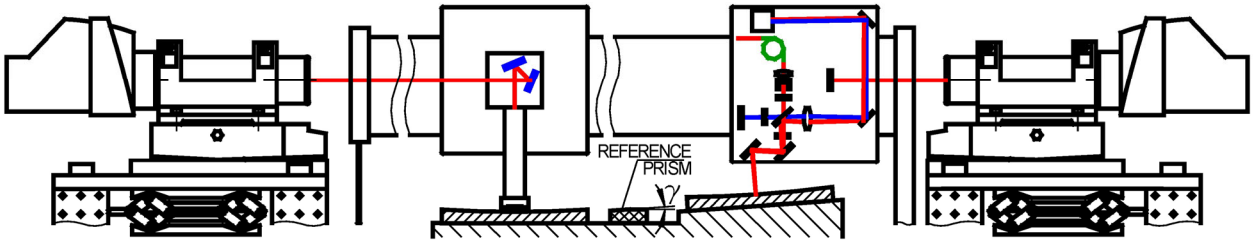

Figure 13. The LTP-2020 experimental arrangement optimized for alignment and measurements with an optical assembly of 1D Wolter Type I optical system consisting of a pair of mirrors, one hyperbolic and one elliptical. The reference prism has two reference surfaces with the relative tilt of γ.

In the LTP-2020 arrangement sketched in Fig. 13, the two sensors are first aligned with a specially developed reference prism with two reference surfaces, one horizontal and other one tilted by 4 degrees. In the case of Fig. 13, the AC based arm is used to align the prism using the horizontal reference surface. After that, the LTP-2020 PBI sensor is aligned orthogonally to the tilted reference surface. With the properly aligned LTP-2020 sensors, it is a straightforward task to measure the mirrors' surface slope distributions, find their optical centers, and set the required relative position and pitch tilt angle. The positioning with sub-micron accuracy can be monitored with the LTP-2020 linear encoders. All these tasks can be performed without an additional realignment between the iterative measurements.

4.2 VLS grating metrology with the LTP-2020

The surface-slope-measuring LTPs remain the preferred tools for x-ray diffraction grating characterization at synchrotron radiation facilities [48-52,107].

The diffraction equation for a grating with varying groove density is:

$$\sin\alpha - \sin\left[\beta + \delta\beta_m(x)\right] = m\lambda g(x), \tag{4}$$

where α is the angle of incidence, calculated from the surface normal and positive at the counterclockwise direction (Fig. 14), β is the diffraction angle, calculated from the surface normal and positive at the clockwise direction, λ is the wavelength of the probe beam light, $g(x) = g_0 + \delta g(x)$ is the groove density distribution in the tangential point with coordinate x, g_0 is the grove density at the grating center $x = 0$, $\delta\beta_m(x)$ is the variation of the diffraction angle for the *m*-th order. For the grating metrology, the LTP is usually arranged in the Littrow configuration, when the directions of the incidence and diffraction beams (the blue traces in Fig. 14) of the selected order coincide for the grating center, $\delta\beta_m(x=0) = 0$. In the perfect Littrow configuration, at $x = 0$, $\alpha_0 = -\beta_0$ (Fig. 14) and Eq. (4) transforms to

$$\sin\beta_0 - \sin\left[\beta_0 + \delta\beta_m(x)\right] = m\lambda \cdot \delta g(x). \tag{5}$$

The LTP grating metrology is aimed at 1D measurements of the diffraction angle variation $\delta\beta_m(x)$ that is a measure of the variation $\delta g(x)$ of the grating's groove density distribution. In many cases, the LTP grating metrology is capable of measuring groove density distributions with the required accuracy. After the upgrade of the ALS XROL LTP-II with a single mode diode laser light source [60], the profiler is also capable of grating metrology [52].

However, in the current LTP-II arrangement, when scanning the optical sensor along the grating under test, there is a measurement error related to carriage wobbling. Together with the surface slope variation, the carriage wobbling leads to the variation of the effective incidence angle in Eq. (4) and an associated error in the measured value of $\delta g(x)$, which is rather difficult to account for [52]. This is because of the transcendental character of the diffraction equations (4) and (5) and an uncertainty of the absolute values of the incident α_0 and diffraction β_0 angles, if special sophisticated absolute angle measuring equipment is not used.

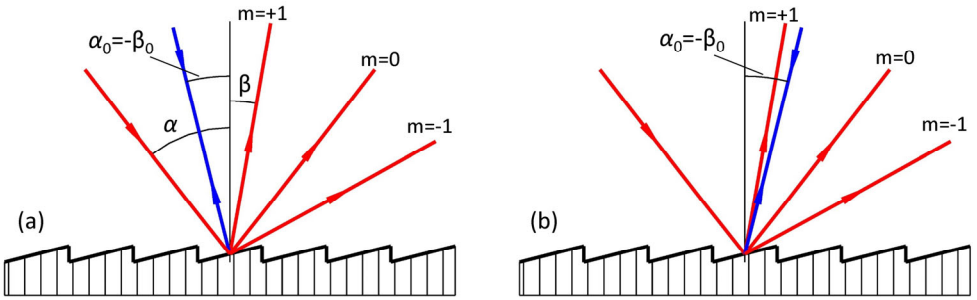

Figure 14: The Littrow configuration arrangement for (a) m = +1 and (b) m = -1 order diffractions. We use here the convention on the incidence α and diffraction β angles as defined in Eq. (4), when the both angles α and β are positive. In the first-order Littrow configurations (the blue coinciding traces of the incidence and diffracted light beams), $\alpha_0 = -\beta_0$

The wobbling error problem in the LTP-II is especially important for a VLS grating with rapid variation of the groove density, such that the overall variation of the diffraction angle surpasses the angular dynamic range of the tool. In this case, to thoroughly characterize the grating, one needs to stitch together multiple overlapped scans, performed with different pitch tilts of the grating. Such stitching requires high-precision absolute measurements of the incidence and diffraction angles for each point of a scan, which is extremely difficult because of the uncertainty in the absolute referencing of the LTP-II angular coordinate system mentioned above. The wobbling error is negligible in the LTP arrangement with a stationary LTP and a movable pentaprism or an adjustable mirror-based folding prism [49-51].

Consequently, one of the major objectives for the development of the LTP-2020 is to enable high accuracy VLS grating metrology. Figure 15 depicts the LTP-2020 VLS grating measurement schematic with stationary sensor and movable folding prism.

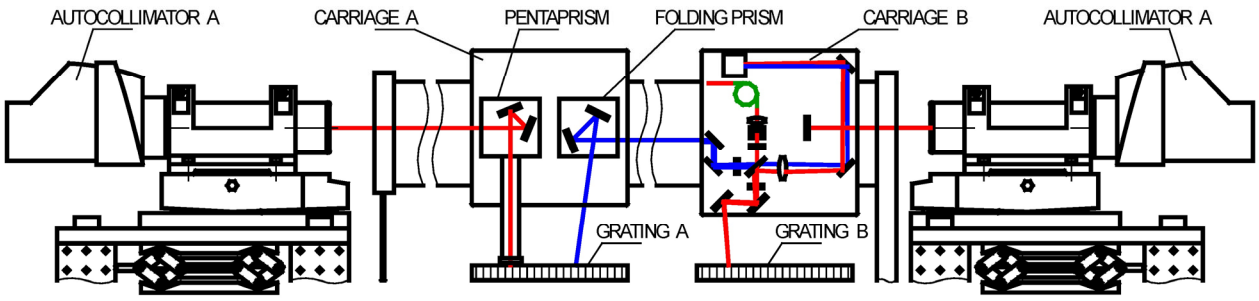

Figure 15. The LTP-2020 experimental arrangement optimized for groove density distribution measurements with x-ray diffraction grating. See text for more details.

In Fig. 15, there are two prisms mounted to the movable carriage A. The movable pentaprism and ELCOMAT 5000 (autocollimator A) are arranged for the zero-order measurement of the surface slope variation of the grating A. Because of the broad-band non-coherent LED light source, the AC based profilers are not capable of grove density measurements. This is performed with the LTP-2020 PBI sensor using the frequency-stabilized SMDL option of the light source (see Sec. 2.3).

In the arrangement of Fig. 15, the two folding mirrors in the reference arm of the stationary LTP PBI sensor direct the beam to the mirror-based folding prism on the movable carriage A. With the folding prism, the beam is aligned to realize the diffraction angle measurements in the Littrow configuration (Fig. 14). By scanning the carriage A, it is possible (with a corresponding synchronization of the data acquisition in the AC and LTP-PBI arms; see also the relevant discussion in Sec. 4.1) to simultaneously measure the grating A in the zero and first diffraction orders.

If the measurements with stitching are required, the realignment of the reference PBI sensor beam with the folding prism within the sensor dynamic range is absolute due to the elimination of the wobbling error. After the realignment, the coordinate system has to be reset, for example, by finding the edges of the grating ruled area.

Note that the option for grating metrology with scanning the LTP-2020 PBI optical sensor is still possible. In this case, the pair of folding mirrors in the main (sample) arm is used to tilt the beam enabling the diffraction angle measurements

in the first-order Littrow configuration with the grating B (Fig. 15). The wobbling angle variation of the carriage B translating in the course of the grating B measurements is recorded with an additional AC (autocollimator B in Fig. 15). This measurement arrangement is basically the same as the one optimized for alignment and measurements with an optical assembly and shown in Fig. 12.

The steep variation of the groove density can lead to a large variation of the optical path within the diffracted LTP light beam, causing a strong interference effect in the beam intensity distribution recorded with the LTP detector [108]. This makes it practically impossible to measure the local diffraction angle with the required accuracy when using the returned diffracted beam image in the regular image processing algorithms (see, for example, Ref. [60] and references therein). If the variation of the interference pattern is not too strong, it can be helpful to use the beam positioning approach and algorithm developed for reprocessing of the AC raw data and outlined in Sec. 3.3, above. This work is in progress at the ALS XROL in collaboration with the Working Group 5.21 Length and Angle Graduations of PTB.

If even with the application of the correlation-based data processing approach, the spurious effects due to intra light-beam diffraction and interference still make accurate metrology of the VLS grating impossible, it is still possible to characterize the grating with interference microscope measurements [109]. This microscopy is complimentary to the LTP metrology by providing a method for the absolute measurement of the grove density, rather than the grove density variation.

Moreover, due to low spatial resolution, the LTP grating metrology is not capable of measuring groove phase coherence, which determines the beamline spectral resolution achievable with the grating. This can be done with application of micro-stitching interference microscope measurements (see, for example, Refs. [108,110-113] and references therein).

5. CONCLUSIONS

We have discussed the current results and status of the ongoing research and development project at the ALS X-Ray Optics Laboratory on the development of a new generation long trace profiler, LTP-2020.

We have described the system design that incorporates different types of surface slope sensors, including a classical pencil beam interferometry sensor with a significantly improved and optimized optical design and a deflectometry sensor based on a customized electronic autocollimator, the ELCOMAT 5000. For the LTP PBI sensor, we have redesigned the multifunctional light beam source, based on a super-luminescent emitting diode and a single-mode laser diode recently implemented in the ALS XROL LTP-II. In the future, we would like to treat the possibility of using the AC as a PBI sensor with external light beams from the SLED and SMLD sources of the LTP PBI sensor.

For the AC-based sensor, we have developed a new data processing algorithm applied to the AC raw image data available from the customized AC. The reprocessing of the AC raw data recorded in the AC deflectometric arrangement with the 2.5 mm diameter aperture allows us to significantly (by a factor of 4-5) reduce the quasi-periodic systematic error.

We have described and discussed a variety of the LTP-2020 operation modes with stationary and/or translated sensors possible due to the two-carriage gantry system with adjustable vertical position. We have presented the LTP-2020 experimental arrangements optimized for measurements with x-ray mirrors, multi-element optical systems, and VLS gratings.

Finally, we have designed the LTP-2020 arrangement that is the most general among the options considered throughout this paper. This arrangement that is principally capable for implementation of all considered application and operation modes is the current optical system specification for the LTP-2020 mechanical design work in progress.

We believe that the results of our investigations are crucial for reaching fundamental metrological limits in deflectometric profilometry using state-of-the-art electronic autocollimators and pencil beam interferometry.

The LTP-2020 design with the two-carriage gantry system, flexible arrangement of the AC and LTP PBI sensors, and an easily reconfigured data acquisition and processing system is a solid platform for future research, development, and implementation of new ideas, methods, and techniques for advancing metrology with x-ray optics. In this respect, we would like also to specially emphasize that the LTP-2020 project is welcome for new idea and collaborations. At the present step of the project, we are especially interested in collaboration on the development and fabrication of the state-of-the-art optical elements and subsystems required for the superior measuring performances of the resulted LTP-2020 system.

ACKNOWLEDGEMENTS

Research at the Advanced Light Source at Lawrence Berkeley National Laboratory is supported by the Office of Science, Office of Basic Energy Sciences, and Material Science Division of the U.S. Department of Energy under Contract No. DE-AC02-05CH11231.

DISCLAIMER

REFERENCES

[1] ALS-U, https://als.lbl.gov/als-u/.

[2] Samoylova, L., Sinn, H., Siewert, F., Mimura, H., Yamauchi, K., and Tschentscher, T., "Requirements on hard X-ray grazing incidence optics for European XFEL: Analysis and simulation of wavefront transformations," Proc. SPIE 7360, 73600E/1-9 (2009); https://doi.org/10.1117/12.822251.

[3] Cocco, D., "Recent Developments in UV optics for ultra-short, ultra-intense coherent light sources," Photonics 2015, 2(1), 40-49 (2015); https://doi.org/10.3390/photonics2010040.

[4] Yamauchi, K., Yabashi, M., Ohashi, H., Koyama, T., and Ishikawa, T., "Nanofocusing of X-ray free-electron lasers by grazing-incidence reflective optics," J. Synchrotron Rad. 22(), 592–598 (2015); http://dx.doi.org/10.1107/S1600577515005093.

[5] Yashchuk, V. V., Goldberg, K. A., Lacey, I., McKinney, W. R., Sanchez del Rio, M., and Padmore, H. A., "Diaboloidal mirrors: Algebraic solution and surface shape approximations," J. Synchrotron Rad. 28(4), 1031-1040 (2021); http://doi.org/10.1107/S1600577521004860.

[6] Sanchez del Rio, M., Goldberg, K. A., Yashchuk, V. V., Lacey, I., and Padmore, H. A., "Simulations of applications using diaboloid mirrors," J. Synchrotron Rad. 28(4), 1041-1049 (2021); https://doi.org/10.1107/S160057752100401X.

[7] Howells, M.R. and Lunt, D., "Design considerations for adjustable-curvature, high-power, x-ray mirrors based on elastic bending," Opt. Eng. 32(8), 1981–1989 (1993); https://doi.org/10.1117/12.146391.

[8] Assoufid, L. and Rabedeau. T., Co-Chairs, "X-ray mirrors," in: X-ray Optics for BES Light Source Facilities, Report of the Basic Energy Sciences Workshop on X-ray Optics for BES Light Source Facilities, D. Mills and H. Padmore, Co-Chairs, pp. 32-43, U.S. Department of Energy, Office of Science, Potomac, MD (March 27-29, 2013); http://science.energy.gov/~/media/bes/pdf/reports/files/BES_XRay_Optics_rpt.pdf.

[9] Sutter, J. P., Alcock, S. G., Nistea, I.-T., Wang, H., and Sawhney, K., "Active and Adaptive X-Ray Optics at Diamond Light Source," Synchrotron Rad. News 35(2), 8-13 (2022); doi: 10.1080/08940886.2022.2058856.

[10] Takacs, P. Z., "X-ray optics metrology," in: Handbook of Optics, 3rd ed., Vol. V, M. Bass, Ed., Chapter 46, McGraw-Hill, New York (2009).

[11] Idir, M. and Yashchuk, V. V., Co-Chairs, "Optical and X-ray metrology," in: X-ray Optics for BES Light Source Facilities, Report of the Basic Energy Sciences Workshop on X-ray Optics for BES Light Source Facilities, D. Mills and H. Padmore, Co-Chairs, pp. 44-55, U.S. Department of Energy, Office of Science, Potomac, MD (March 27-29, 2013); http://science.energy.gov/~/media/bes/pdf/reports/files/BES_XRay_Optics_rpt.pdf.

[12] Sutter, J. P., Alcock, S. G., and Sawhney, K., "Measurement and analysis of active synchrotron mirrors under operating conditions," Nucl. Instrum. Methods A710, 72–77 (2013); http://dx.doi.org/10.1016/j.nima.2012.10.115.

[13] Church, E. L., Takacs, P. Z., "Use of an optical profiling instrument for the measurement of the figure and finish of optical quality surfaces," Wear 109, 241-57 (1986).

[14] Takacs, P. Z., Qian, S., and Colbert, J., "Design of a long trace surface profiler," Proc. SPIE 749, 59-64 (1987); https://doi.org/10.1117/12.939842.
[15] Takacs, P. Z., Feng, S. K., Church, E. L., Qian, S., and Liu, W-M., "Long trace profile measurements on cylindrical aspheres," Proc. SPIE 966, 354-64 (1989); https://doi.org/10.1117/12.948082.
[16] Rommeveaux, A., Hignette, O., Morawe, C., "Mirror metrology and bender characterization at ESRF," Proc. SPIE 5921, 59210N/1-8 (2005).
[17] Thomasset M., and Polack, F., "Characterization of optical surfaces for the present generations of synchrotron sources," Proc. SPIE 7155, 715506/1-12 (2008).
[18] Kirschman, J. L., Domning, E. E., McKinney, W. R., Morrison, G. Y., Smith, B. V., and Yashchuk, V. V., "Performance of the upgraded LTP-II at the ALS Optical Metrology Laboratory," Proc. SPIE 7077, 70770A/1-12 (2008).
[19] Rommeveaux, A., Thomasset, M., and Cocco, D., "The Long Trace Profilers," in [Modern Developments in X-ray and Neutron Optics], A. Erko, M. Idir, T. Krist, A. G. Michette, Eds., Chapter 10, Springer-Verlag, Berlin/Heidelberg (2008).
[20] Senba, Y., Kishimoto, H., Ohashi, H., Yumoto, H., Zeschke, T., Siewert, F., Goto, S., and Ishikawa, T., "Upgrade of long trace profiler for characterization of high-precision X-ray mirrors at SPring-8," Nucl. Instr. and Meth. A 616(2-3), 237-240 (2010).
[21] Nikitin, S. M., Gevorkyan, G. S., McKinney, W. R., Lacey, I., Takacs, P. Z., and Yashchuk, V. V., "New twist in the optical schematic of surface slope measuring long trace profiler," Proc. SPIE 10388, 103850I-1-17 (2017); doi: 10.1117/12.2274400.
[22] Yashchuk, V. V., Rochester, S., Lacey, I., and Babin, S., "Super-resolution surface slope metrology of x-ray mirrors," Rev. Sci. Instrum. 91, 075113/1-11 (2020); doi: 10.1063/5.0005556.
[23] Centers, G., Smith, B. V., and Yashchuk, V. V., "New operational mode of the pencil beam interferometry based LTP," Proc. SPIE 9962, 996202/1-13 (2016); https://doi.org/10.1117/12.2238298.
[24] Siewert, F., Noll, T., Schlegel, T., Zeschke, T., and Lammert, H., "The Nanometre Optical Component Measuring Machine: a new Sub-nm Topography Measuring Device for X-ray Optics at BESSY," AIP Conference Proceedings 705, 847-850 (2004).
[25] Siewert, F., Buchheim, J., Zeschke, T., Störmer, M., Falkenberg, G., and Sankari, R., "On the characterization of ultra-precise X-ray optical components: advances and challenges in ex situ metrology," J. Synchrotron Rad. 21, 968–975 (2014); doi: 10.1107/S1600577514016221.
[26] Yashchuk, V. V., Barber, S., Domning, E. E., Kirschman, J. L., Morrison, G. Y., Smith, B. V., Siewert, F., Zeschke, T., Geckeler, R., and Just, A., "Sub-microradian surface slope metrology with the ALS Developmental Long Trace Profiler," Nucl. Instr. and Meth. A 616(2-3), 212-223 (2010).
[27] Alcock, S. G., Sawhney, K. J. S., Scott, S., Pedersen, U., Walton, R., Siewert, F., Zeschke, T., Senf, F., Noll, T., and Lammert, H., "The Diamond-NOM: A non-contact profiler capable of characterizing optical figure error with sub-nanometre repeatability," Nucl. Instr. Meth. A 616(2-3), 224-228 (2010).
[28] Qian, J., Sullivan, J., Erdmann, M., Khounsary, A., and Assoufid, L., "Performance of the APS optical slope measuring system," Nucl. Instrum. and Meth. A 710, 48–51 (2013); https://doi.org/10.1016/j.nima.2012.10.102.
[29] Nicolas, J. and Martınez, J. C., "Characterization of the error budget of Alba-NOM," Nucl. Instr. and Meth. A 710, 24-30 (2013).
[30] Lacey, I., Artemiev, N. A., Domning, E. E., McKinney, W. R., Morrison, G. Y., Morton, S. A., Smith, B. V., and Yashchuk, V. V., "The developmental long trace profiler (DLTP) optimized for metrology of side-facing optics at the ALS," Proc. SPIE 9206, 920603/1-11 (2014); doi:10.1117/12.2061969.
[31] Qian, S., Geckeler, R. D., Just, A., Idir, M., and Wu, X., "Approaching sub-50 nanoradian measurements by reducing the saw-tooth deviation of the autocollimator in the Nano-Optic-Measuring Machine," Nucl. Instr. and Meth. A 785, 206-212 (2015).
[32] Lacey, I., Anderson, K., Centers, G. P., Geckeler, R. D. Gevorkyan, G. S., Just, A., Nicolot, T., Smith, B. V., and Yashchuk, V. V., "The ALS OSMS: Optical Surface Measuring System for high accuracy two-dimensional slope metrology with state-of-the-art x-ray mirrors," Proc. SPIE 10760, 1076002 (2018); https://doi.org/10.1117/12.2321347.
[33] Assoufid, L., Bray, M., Qian, J., and Shu, D., "3-D surface profile measurements of large x-ray synchrotron radiation mirrors using stitching interferometry," Proc. SPIE 4782 21-28 (2002); https://doi.org/10.1117/12.454816.

[34] Mimura, H., Yumoto, H., Matsuyama, S., Yamamura, K., Sano, Y., Ueno, K., Endo, K., Mori, Y., Yabashi, M., Tamasaku, K., Nishino, Y., Ishikawa, T., and Yamauchi, K., "Relative angle determinable stitching interferometry for hard x-ray reflective optics," Rev. Sci. Instrum. 76, 045102 (2005); https://doi.org/10.1063/1.1868472.
[35] Assoufid, L., Qian, J., Kewish, C., Liu, C., Conley, R., Macrander, A. T., Lindley, D., and Saxer, C., "A Microstitching Interferometer for Evaluating the Surface Profile of Precisely Figured Hard X-ray K-B Mirrors," Proc. of SPIE 6704, 670406/1-12 (2007); doi: 10.1117/12.736384.
[36] Yumoto, H., Mimura, H., Kimura, T., Handa, S., Matsuyama, S., Sano, Y., and Yamauchi, K., "Stitching interferometric metrology for steeply curved x-ray mirrors," Surface and Interface Analysis 40(6-7), 1023-1027 (2008); https://doi.org/10.1002/sia.2807.
[37] Ludbrook, G. D., Alcock, S. G., and Sawhney, K. J. S., "A Fizeau interferometer system with double-pass and stitching for characterizing the figure error of large (> 1m) synchrotron optics," Proc. SPIE 7389, 738939 (2009).
[38] Vivo, A., Lantelme, B., Baker, R., and Barrett, R., "Stitching methods at the European Synchrotron Radiation Facility (ESRF)," Rev. Sci. Instrum. 87, 051908 (2016); https://doi.org/10.1063/1.4950745.
[39] Yumoto, H., Koyama, T., Matsuyama, S., Yamauchi, K., and Ohashi, H., "Stitching interferometry for ellipsoidal x-ray mirrors," Rev. Sci. Instrum. 87, 051905 (2016); https://doi.org/10.1063/1.4950714.
[40] Vivo, A. and Barrett, R., "Fizeau stitching at the European synchrotron radiation facility (ESRF)," Proc. SPIE 10385, 103850N (2017).
[41] Vivo, A., Barrett, R., and Perrin, F., "Stitching techniques for measuring X-ray synchrotron mirror topography," Rev. Sci. Instrum. 90, 021710 (2019); https://doi.org/10.1063/1.5063339.
[42] Huang, L., Wang, T., Tayabaly, K., Kuhne, D., Weihe Xu, Wei Xu, Vescovi, M., and Idir, M., "Stitching interferometry for synchrotron mirror metrology at National Synchrotron Light Source II (NSLS-II)," Optics and Lasers in Engineering 124, 105795/1-9 (2020); https://doi.org/10.1016/j.optlaseng.2019.105795.
[43] Shahinian, H., Hovis, C., and Evans, C., "The effect of retrace error on stitching coherent scanning interferometry measurements of freeform optics," Opt. Express 29(18), 28562- 28573 (2021); doi: 10.1364/OE.433435.
[44] von Bieren, K., "Pencil Beam Interferometer For Aspherical Optical Surfaces," Proc. SPIE 343, 101-108 (1982); https://doi.org/10.1117/12.933743.
[45] von Bieren, K., "Interferometry of wave fronts reflected off conical surfaces," Appl. Opt. 22, 2109-2114 (1983); https://doi.org/10.1364/AO.22.002109.
[46] von Bieren, K., "Pencil beam interferometer," US Patent 4,498,773 (1985).
[47] MÖLLER-WEDEL OPTICAL, GmbH, [ELCOMAT 3000 Electronic Autocollimator]; https://www.haag-streit.com/moeller-wedel-optical/products/electronic-autocollimators/elcomat-product-line/elcomat-3000/.
[48] Irick, S. C. and McKinney, W. R., "Measurement of diffraction gratings with a long trace profiler with application for synchrotron beamline gratings," AIP Conf. Proc. 417, 118–123 (1997); ttps://doi.org/10.1063/1.54581.
[49] Cocco, D., Sostero, G., and Zangrando, M., "Technique for measuring the groove density of diffraction gratings using the long trace profiler," Rev. Sci. Instrum. 74(7), 3544-3548 (2003); https://doi.org/10.1063/1.1584080.
[50] Siewert, F., Lammert, H., Reichardt, G., Hahn, U., Treusch, R., and Reininger, R., "Inspection of a spherical triple VLS-grating for self-seeding of FLASH at DESY," AIP Conf. Proc. 879, 667-670 (2007); https://doi.org/10.1063/1.2436150.
[51] Thomasset, M., Dvorak, J., Brochet, S., Dennetiere, D., and Polack, F., "Grating metrology for X-ray and V-UV synchrotron beamlines at SOLEIL," Rev. Sci. Instrum. 90(2), 021714 (2019); https://doi.org/10.1063/1.5055284.
[52] Lacey, I. and Yashchuk, V. V., "Characterization of Groove Density Variation of VLS gratings with ALS XROL LTP-II in different operation modes," Proc. SPIE 11492, 114920D/1-16 (2020); doi: 10.1117/12.2568705.
[53] Yashchuk, V. V., Artemiev, N. A., Lacey, I., McKinney, W. R., and Padmore, H. A., "Advanced environmental control as a key component in the development of ultra-high accuracy ex situ metrology for x-ray optics," Opt. Eng. 54(10), 104104/1-14 (2015); doi: 10.1117/1.OE.54.10.104104.
[54] ALS-U Project at Lawrence Berkeley National Lab, Overview; https://als.lbl.gov/als-u/overview/.
[55] Kevan, S., Chair, [ALS-U: Solving Scientific Challenges with Coherent Soft X-Rays], Workshop report on early science enabled by the Advanced Light Source Upgrade, ALS, LBNL, Berkeley, CA, (2017) https://als.lbl.gov/wp-content/uploads/2017/08/ALS-U-Early-Science-Workshop-Report-Full.pdf.
[56] Takacs, P. Z., Lacey, I., and Yashchuk, V. V., "Raytracing the Long Trace Profiler," Proc. SPIE 11492, 1149204/1-22 (2020); doi: 10.1117/12.2569751.
[57] Takacs, P. Z., Lacey, I., and Yashchuk, V. V., "Optimized design of the ALS LTP-2020 using geometrical and physical optics raytracing," Invited talk at the 7th International Workshop on X-ray Optics and Metrology, The SRI2022 Satellite Workshop (IWXM 2022) (Berlin, Germany, April 5, 2022).

[58] Takacs, P. Z., Lacey, I., and Yashchuk, V. V., "Towards a new generation long trace profiler LTP-2020: Optical design of pencil beam interferometry sensor," Abstract to SPIE Optics and Photonics 2023, Conference Advances in Metrology for X-Ray and EUV Optics X (San Diego, August 20-24, 2023), Paper No.: OP501-11; Tracking No.: OP23O-OP501-11; this conference.
[59] Geckeler, R. D., Just, A., Krause, M., Schnabel, O., Lacey, I., English, D., and Yashchuk, V. V., "Self-calibration strategies for reducing systematic slope measurement errors of autocollimators in deflectometric profilometry," Abstract to the Metrology, Astronomy, Diagnostics and Optics Workshop (MEADOW-2023), Trieste, Italy, September 12-14, 2023.
[60] Yashchuk, V. V., Lacey, I., Anderson, K., Dickert, J., Smith, B. V., and Takacs, P. Z., "Multifunctional light beam source for surface slope measuring long trace profilers," Proc. SPIE 11492, 1149205/1-18 (2020); doi: 10.1117/12.2570462.
[61] Lacey, I., Anderson, K., Dickert, J., Nelson, B., Takacs, P. Z., and Yashchuk, V. V., "Development of an advanced LTP at the ALS: Operation and data acquisition with a two-carriage gantry system," Poster presentation at the 7th International Workshop on X-ray Optics and Metrology, The SRI2022 Satellite Workshop (IWXM 2022) (Berlin, Germany, April 6, 2022).
[62] Lacey, I., Anderson, K., Dickert, J., English, D., Nelson, B., Takacs, P. Z., and Yashchuk, V. V., "Towards a new generation long trace profiler LTP-2020: Design, motion control, and performance of a two-carriage gantry system," Abstract to SPIE Optics and Photonics 2023, Conference Advances in Metrology for X-Ray and EUV Optics X (San Diego, August 20-24, 2023), Paper No.: OP501-15; Tracking No.: OP23O-OP501-15; this conference.
[63] MÖLLER-WEDEL OPTICAL, GmbH, [ELCOMAT 5000 Electronic Autocollimator]; https://www.haag-streit.com/fileadmin/Moeller_wedel_optical/Brochures/Electronic_Autocollimators/ELCOMAT_5000_Brochure.pdf.
[64] Irick, S. C., McKinney, W. R., Lunt, D. L. T., and Takacs, P. Z., "Using a straightness reference in obtaining more accurate surface profiles," Rev. Sci. Instrum. 63, 1436–1438 (1992); https://doi.org/10.1063/1.1143036.
[65] Irick, S. C., "Improved measurement accuracy in a long trace profiler: compensation for laser pointing instability," Nucl. Instrum. Methods Phys. Res. A 347, 226–230 (1994); https://doi.org/10.1016/0168-9002(94)91882-1.
[66] Li, H., Takacs, P. Z., and Oversluizen, T., "Vertical scanning long trace profiler: a tool for metrology of x-ray mirrors," Proc. SPIE 3152, 180–187 (1997); https://doi.org/10.1117/12.295557.
[67] Takacs, P. Z., Church, E. L., Bresloff, C. J., Assoufid, L., "Improvements in the accuracy and the repeatability of long trace profiler measurements," Appl. Optics 38(25), 5468-5479 (1999); https://doi.org/10.1364/AO.38.005468.
[68] Yashchuk, V. V., "Optimal Measurement Strategies for Effective Suppression of Drift Errors," Rev. Sci. Instrum. 80, 115101-1-10 (2009); http://dx.doi.org/10.1063/1.3249559.
[69] Yashchuk, V. V., Centers, G., Gevorkyan, G. S., Lacey, I., and Smith, B. V., "Correlation methods in optical metrology with state-of-the-art x-ray mirrors," Proc. SPIE 10612, 106120O (2018); https://doi.org/10.1117/12.2305441.
[70] Siewert, F., Buchheim, J., Höft, T., Zeschke, T., Schindler, A., and Arnold, T., "Investigations on the spatial resolution of autocollimator-based slope measuring profilers," Nucl. Instrum. Methods A 710, 42–47 (2013); https://doi.org/10.1016/j.nima.2012.10.130.
[71] Siewert, F., Zeschke, T., Arnold, T., Paetzeld, H., and Yashchuk, V. V., "Linear chirped slope profile for spatial calibration in slope measuring deflectometry," Rev. Sci. Instrum. 87(5), 051907/1-8 (2016); https://doi.org/10.1063/1.4950737.
[72] Yashchuk, V. V., Lacey, I., Arnold, T., Paetzelt, H., Rochester, S., Siewert, F., and Takacs, P. Z., "Investigation on lateral resolution of surface slope profilers," Proc. SPIE 11109, 111090M/1-19 (2019); doi: 10.1117/12.2539527.
[73] Takacs, P. Z., and Qian, S., "Accuracy Limitations in Long-Trace Profilometry," AIP Conference Proceedings, 705 (1), pp. 831-834 (2004) doi: 10.1063/1.1757924. See page 4.
[74] Faustini, L., and Martini, G., "Bend loss in single-mode fibers," J. Lightwave Tech. 15(4), 671-679 (1997); doi: 10.1109/50.566689.
[75] Smink, R. W., de Hon, B. P., and Tijhuis, A.G., "Bend-induced loss in single-mode fibers," Proc. Symposium IEEE/LEOS Benelux Chapter, 2005, p.p. 281-284; http://www.photonics-benelux.org/images/stories/media/proceedings/2005/s05p281.pdf.
[76] Bristol Instruments 671 Series Laser Wavelength Meter Model 671B-VIS; http://www.bristol-inst.com/products/wavelengthmeters -scientific/671-series-CW-lasers.
[77] Teledyne Photometrics, "KINETIX;" https://www.photometrics.com/products/kinetix-family/kinetix

[78] Lacey, I., Adam, J., Centers, G., Gevorkyan, G. S., Nikitin, S. M., Smith, B. V., and Yashchuk, V. V., "Development of a high performance surface slope measuring system for two-dimensional mapping of x-ray optics," Proc. SPIE 10385, 103850G-1-13 (2017); doi: 10.1117/12.2273029.
[79] Lacey, I., Geckeler, R. D., Just, A., Siewert, F., Arnold, T., Paetzelt, H., Smith, B. V., and Yashchuk, V. V., "Optimization of size and shape of aperture in autocollimator-based deflectometric profilometers," Rev. Sci. Instrum. 90(2), 021717/1-14 (2019); doi: 10.1063/1.5058710.
[80] Probst, R., Wittekopf, R., Krause, M., Dangschat, H., and Ernst, A., "The new PTB angle comparator," Meas. Sci. Technol. 9, 1059 – 1066 (1998); doi: 10.1088/0957-0233/9/7/009.
[81] Just, A., Krause, M. Probst, R., Bosse, H., Haunerdinger, H., Spaeth, C., Metz, G., and Israel, W., "Comparison of angle standards with the aid of a high-resolution angle encoder," Precis. Eng. 33(4), 530-3 (2009); doi: 10.1016/J.PRECISIONENG.2009.02.004.
[82] Geckeler, R. D., Link, A., Krause, M., and Elster, C., "Capabilities and limitations of the self-calibration of angle encoders," Meas. Sci. Technol. 25, 055003/1-10 (2014); doi:10.1088/0957-0233/25/5/055003.
[83] Geckeler, R. D. and Just, A., "Optimized use and calibration of autocollimators in deflectometry," Proc. SPIE 6704, 670407/1-12 (2007); https://doi.org/10.1117/12.732384.
[84] Siewert, F., Buchheim, J., and Zeschke, T., "Characterization and calibration of 2nd generation slope measuring profiler," Nucl. Instrum. Meth. A 616(2-3), 119–127 (2010); doi: 10.1016/j.nima.2009.12.033.
[85] Geckeler, R. D., Artemiev, N. A., Barber, S. K., Just, A., Lacey, I., Kranz, O., Smith, B. V., and Yashchuk, V. V., "Aperture alignment in autocollimator-based deflectometric profilometers," Rev. Sci. Instrum. 87(5), 051906/1-8 (2016); doi: 10.1063/1.4950734.
[86] Geckeler, R. D. and Just, A., "A shearing-based method for the simultaneous calibration of angle measuring devices," Meas. Sci. and Tech. 25, 105009 (2014); DOI: 10.1088/0957-0233/25/10/105009.
[87] Geckeler, R. D., Křen, P., Just, A., Schumann, M., Krause, M., and Yashchuk, V. V., "Environmental influences on autocollimator-based angle and form metrology," Rev Sci. Instrum. 90(2), 021705/1-15 (2019); doi: 10.1063/1.5057402.
[88] Nicolas, J., Pedriera, J., Sics, I., Ramirez, C., and Campos, J., "Nanometer accuracy with continuous scans at the ALBA-NOM," Proc. SPIE 9962, Advances in Metrology for X-Ray and EUV Optics VI, 996203 (2016); doi:10.1117/12.2238128.
[89] Geckeler, R. D., Just, A., Schumann, M., Krause, M., Lacey, I., and Yashchuk, V. V., "In pursuit of fundamental limits in deflectometric form measurement: Current status and future challenges," Invited talk at the 7th International Workshop on X-ray Optics and Metrology, The SRI2022 Satellite Workshop (IWXM 2022) (Berlin, Germany, April 5, 2022).
[90] Debler, E. and Zander, K., "Measurement of evenness on optical plane surfaces with autocollimator and pentagon prism," PTB-Mitteilungen 90(5), 339-349 (1980).
[91] Qian, S., Jark, W., and Takacs, P. Z., "The penta-prism LTP: A long-trace-profiler with stationary optical head and moving penta prism," Rev. Sci. Instrum. 63(3), 2562-2569 (1995); https://doi.org/10.1063/1.1145658.
[92] Barber, S. K., Morrison, G. Y., Yashchuk, V. V., Gubarev, M. V., Geckeler, R. D., Buchheim, J., Siewert, F., and Zeschke, T., "Developmental long trace profiler using optimally aligned mirror based pentaprism," Opt. Eng. 50(5), 053601-1-10 (2011); https://doi.org/10.1117/1.3572113.
[93] Barber, S. K., Geckeler, R. D., Yashchuk, V. V., Gubarev, M. V., Buchheim, J., Siewert, F., and Zeschke, T., "Optimal alignment of mirror based pentaprism for scanning deflectometric devices," Opt. Eng. 50(7), 073602/1-8 (2011); https://doi.org/10.1117/1.3598325.
[94] Yashchuk, V. V. "Sub-microradian Surface Slope Metrology at the ALS Optical Metrology Laboratory and around the World," Oral presentation at the First Meeting on Development of a New Optical Surface Slope Measuring System - OSMS-I (ALS, Berkeley, March 26, 2010).
[95] Qian, S. N. and Idir, M., "Innovative nano-accuracy surface profiler for sub-50 nrad rms mirror test," Proc. SPIE 9687, 96870D-1-10 (2016); doi: 10.1117/12.2247575.
[96] Cocco, D., Idir, M., Morton, D., Raimondi, L., and Zangrando, M., "Advances in X-ray optics: From metrology characterization to wavefront sensing-based optimization of active optics," Nucl. Instum. and Meth. A 907, 105–115 (2018); https://doi.org/10.1016/j.nima.2018.03.026.
[97] Huang, L., Wang, T., Nicolas, J., Polack, F., Zuo, C., Nakhoda, K., and Idir, M., "Multi-pitch self-calibration measurement using a nano-accuracy surface profiler for X-ray mirror metrology," Opt. Express 28(16), 23060-(2020); doi: 10.1364/OE.392433.

[98] Yashchuk, V. V., McKinney, W. R., Warwick, T., Noll, T., Siewert, F., Zeschke, T., and Geckeler, R. D., "Proposal for a Universal Test Mirror for Characterization of Slope Measuring Instruments," Proc. SPIE 6704, 67040A/1-12 (2007); doi:10.1117/12.732719.
[99] Yashchuk, V. V., Artemiev, N. A., Centers, G., Chaubard, A., Geckeler, R. D., Lacey, I., Marth, H., McKinney, W. R., Noll, T., Siewert, F., Winter, M., and Zeschke, T., "High precision tilt stage as a key element to universal test mirror for characterization and calibration of slope measuring instruments," Rev. Sci. Instrum. 87(5), 051904 (2016); doi: 10.1063/1.4950729.
[100] Ali, Z., Artemiev, N. A., Cummings, C. L., Domning, E. E., Kelez, N., McKinney, W. R., Merthe, D. J., Morrison, G. Y., Smith, B. V., and Yashchuk, V. V., "Automated suppression of errors in LTP-II slope measurements with x-ray optics," Proc. SPIE 8141, 81410O-1-15 (2011); http://dx.doi.org/10.1117/12.894061.
[101] Geckeler, R. D., Yashchuk, V. V., and Lacey, I., "Improvement of the angle measurement of autocollimators by use of advanced algorithms for the analysis of the reticle images and multiple approaches to error compensation: Part 1: Ideas, algorithms, and experimental validation," Advanced Light Source Beam Line Note LSBL-1505 (February 15, 2023), ALS LBNL, Berkeley, CA, USA (available upon a direct request).
[102] Just, A., Krause, M., Probst, R., and Wittekopf, R., "Calibration of high-resolution electronic autocollimators against an angle comparator," Metrologia 40, 288-294 (2003); doi: 10.1088/0957-0233/25/1/015010.
[103] Wolter, H., "Glancing Incidence Mirror Systems as Imaging Optics for X-rays," Annalen der Physik. 6th Ser. 10, 94 (1952); doi:10.1002/andp.19524450108.
[104] Wolter, H., "A Generalized Schwarzschild Mirror System For Use at Glancing Incidence for X-ray Imaging," Annalen der Physik. 6th Ser. 10, 286 (1952); doi:10.1002/andp.19524450410.
[105] Chuang, Y.-D., Anderson, C. N., Benk, M. P., Goldberg, K. A., Voronov, D. L., Warwick, T., Yashchuk, V. V., and Padmore, H. A., "Multiplexed high resolution soft x-ray RIXS," SRI 2015, AIP Conf. Proc. 1741, 050011-1-5 (2016); http://dx.doi.org/10.1063/1.4952931.
[106] Yashchuk, V. V., Lacey, I., Gevorkyan, G. S., McKinney, W. R., Smith, B. V., and Warwick, T., "Ex situ metrology and data analysis for optimization of beamline performance of aspherical pre-shaped x-ray mirrors at the Advanced Light Source," Rev. Sci. Instrum. 90(2), 021711/1-13 (2019); doi: 10.1063/1.5057441.
[107] Cocco, D., and Thomasset, M., "Measurement of groove density of diffraction gratings," in: [Modern Developments in X-Ray and Neutron Optics], Springer-Verlag, 2008, pp. 207–211, ISBN: 978-3-540-74560-0.
[108] Rochester, S., English, D., Lacey, I., Munechika, K., and Yashchuk, V. V., "Towards super-resolution interference microscopy metrology of x-ray variable-line-spacing diffraction gratings: Recent Developments," SPIE Proc. 12240, 122400E/1-14 (2022); doi: 10.1117/12.2633637.
[109] Yashchuk, V. V., McKinney, W. R., Artemiev, N. A., "Ex situ metrology of x-ray diffraction gratings," Nucl. Instrum. Meth. A710, 59–66 (2013); https://doi.org/10.1016/j.nima.2012.10.109.
[110] Yamauchi, K., Yamamura, K., Mimura, H., Sano, Y., Saito, A., Ueno, K., Endo, K., Souvorov, A., Yabashi, M., Tamasaku, K., Ishikawa, T., and Mori, Y., "Microstitching interferometry for x-ray reflective optics," Rev. Sci. Instrum. 74(5), 2894–2898 (2003); https://doi.org/10.1063/1.1569405.
[111] Vivo A. and Barrett, R., "Micro-stitching interferometry at the ESRF," Nucl. Instrum. and Meth. A616, 183–187 (2010); doi: 10.1016/j.nima.2009.11.073.
[112] Yumoto, H., Mimura, H., Handa, S., Kimura, T., Matsuyama, S., Sano, Y., Ohashi, H., Yamauchi, K., and Ishikawa, T., "Stitching-angle measurable microscopic-interferometer: Surface-figure metrology tool for hard X-ray nanofocusing mirrors with large curvature," Nucl. Instrum. and Meth. A 616, 203-206 (2010); doi: 10.1016/j.nima.2009.11.073.
[113] Thomasset, M., Idir, M., Polack, F., Bray, M., and Servant, J.-J., "A new phase-shift microscope designed for high accuracy stitching interferometry," Nucl. Instrum. and Meth. A 710, 7–12 (2013).